NASA CONTRACTOR REPORT

NASA CR-351

NASA CR-351

RESEARCH ON AN EXPANDABLE AIRLOCK UTILIZING THE ELASTIC RECOVERY PRINCIPLE

by N. O. Brink

Prepared under Contract No. NAS 7-283 *by*
WHITTAKER CORPORATION
San Diego, Calif.
for Western Operations Office

NATIONAL AERONAUTICS AND SPACE ADMINISTRATION • WASHINGTON, D. C. • DECEMBER 1965

NASA CR-351

RESEARCH ON AN EXPANDABLE AIRLOCK UTILIZING THE ELASTIC RECOVERY PRINCIPLE

By N. O. Brink

Prepared under Contract No. NAS 7-283 by
WHITTAKER CORPORATION
San Diego, Calif.

for Western Operations Office

NATIONAL AERONAUTICS AND SPACE ADMINISTRATION

For sale by the Clearinghouse for Federal Scientific and Technical Information
Springfield, Virginia 22151 – Price $4.00

FOREWORD

This report was prepared by Whittaker Corporation, Narmco Research & Development Division, under Contract No. NAS7-283, entitled "Research on an Expandable Airlock Utilizing the Elastic Recovery Principle." The work was accomplished under the overall management of Mr. Norman J. Mayer, Chief, Structures Research Branch, Office of Advanced Research and Technology, National Aeronautics and Space Administration Headquarters. The technical monitor for this program was Mr. Robert S. Osborne, Space Station Research Group, NASA-Langley Research Center, with Mr. Jerry G. Williams acting as project engineer.

Mr. B. L. Duft, Manager, Engineering Department, Narmco Research & Development Division, was in charge of the basic research and development work. The program was accomplished under the direction of Mr. R. Hidde, Chief, Project Engineering, with Mr. N. O. Brink designated as project engineer. The major contributors to this program were Messrs. C. E. Thompson, Senior Research Engineer; S. I. Feher, Research Engineer, and S. Yagi, Senior Design Engineer.

A major subcontract was awarded to Astro Research Corporation, Santa Barbara, California, to perform the development and analytical work for structural fabric of the airlock design.

ABSTRACT

This Final Report describes work on a program whose objective was to determine the feasibility of designing an expandable airlock utilizing elastic recovery materials. The airlock design criteria included requirements for easy crew transfer, micrometeoroid and thermal protection, maximal flexibility, multiple deployment – retraction cycles, and minimal leakage. The criteria resulted in an expandable airlock design approximately 4 ft in diameter and 7 ft long with a total system weight of 101 lb.

The design of the expandable airlock was accomplished in accordance with all protective, structural, and operational requirements. The shape of the structural fabric was based on isotensoid characteristics. This design approach provides convolutions in the composite wall, which also improves packaging and folding characteristics. The operational requirements suggest the use of cables to retract the airlock for storage during periods when the structure is not in use; the system design defines a mechanism utilizing this means of retraction. Analysis has shown that the elastic recovery layers would provide the necessary protection against space hazards when the airlock was deployed.

This study has indicated that an expandable airlock using elastic recovery materials is definitely feasible; Narmco therefore recommends that fabrication of a complete test system be initiated.

TABLE OF CONTENTS

Section		Page
I	Introduction	1
II	Design Criteria	3
III	Materials	4
	A. Thermal Control Surface	4
	B. Materials for Micrometeoroid Protection	4
	C. Selection of Filamentary Materials	6
	D. Liner Material	6
IV	Expandable Airlock Thermal Analysis	12
	A. Nomenclature	12
	B. Discussion	13
	C. Critical Design Conditions	14
	D. Radiation Heat Exchange between the Airlock and the Space Vehicle	15
	E. Vehicle Orientation for Maximal Heating	20
	F. Thermal Balance and Temperature Determination	23
	G. Computer Solution	28
	H. Results and Conclusions	28
V.	Design of Structural Fabric	41
	A. Types of Structural Fabrics	41
	B. Structural Analysis	43
	C. Design Data for Airlock Structure	50
	D. General Dimensions for Airlock Structure	50
	E. Detail Design for Airlock Structure	55

TABLE OF CONTENTS (Continued)

Section		Page
VI	Meteoroid Protection for the Expandable Airlock	60
	A. Introduction	60
	B. Analysis	60
	C. Discussion	68
VII	Radiation Protection	69
VIII	Folding and Packaging	71
	A. Packaging Capabilities	81
IX	Design of Airlock	83
	A. Attachments	83
	B. Rim	83
	C. Hatch	86
	D. Retraction Mechanism	87
	E. Inner Liner	87
X	Weight Estimate	88
XI	Conclusions and Recommendations	90
	References	91

LIST OF FIGURES

Figure		Page
1	Expandable Airlock	2
2	Flexible Elastic Recovery Materials	7
3	Liner Test Fixture	11
4	Form Factor Notation	16
5	Finite Difference Form Factor Notation	18
6	Projected Area Geometry	21
7	Octagonal Model of Airlock	24
8	Heat Transfer through the Vehicle Wall	27
9	External Surface Temperatures	32
10	Internal Temperatures	33
11	External Surface Temperature	34
12	Internal Temperatures	35
13	External Surface Temperatures	36
14	Internal Temperatures	37
15	External Surface Temperatures	38
16	Internal Temperatures	39
17	General Shape of Airlock Structure	42
18	Combined Knitting and Filament-Wound Structures	44
19	Equilibrium Conditions on Longitudinal Fiber	45
20	Effect of Outside Diameter on Tube Length	47
21	Equilibrium for a Hoop	48
22	Rim and Drawstring Forces	49
23	General Arrangement of Airlock Structure	51
24	Cross-Sectional Detail for Hoop.	57

LIST OF FIGURES (Continued)

Figure		Page
25	Cross-Sectional Detail for Drawstring	58
26	Cylindrical Model in Fixture	72
27	Cylindrical Cylinder with Flexible Bands	74
28	Folding Sequence for the Cylinder with "Flexible" Bands	75
29	Corrugated Cylinder without Bands	76
30	Cylinder Model with Rigid Hoop Rings	77
31	Large Test Cylinder, 4-ft Diameter and 3 ft Long	78
32	Large Cylinder with Buckling Failure on Initial Test	78
33	Load-Deformation Curve for 4-ft Diameter Cylinder	79
34	Large Cylinder with Vertical Supports at Maximum Load	80
35	Expandable Airlock General Design Concept	84
36	Cross-Sectional Detail for Rim	85

LIST OF TABLES

Table		Page
1	Design Criteria for the Expandable Airlock	3
2	Candidate Matrix Materials	5
3	Mechanical Properties of Filaments	8
4	Permeability of Film Materials	10
5	Computer Input Data	29
6	Summary of Computer Analysis; Maximal Heating Condition	31
7	Effective Atomic Number and Density of Elastic Recovery Materials	70
8	Packaging Ratio for Airlock Type Structures	82
9	Airlock Weight Estimate	89

I. INTRODUCTION

The elastic recovery concept is a mechanism by which a flexible structure may be erected in space. This concept is particularly well suited to an expandable airlock, as it provides a wall which is self-erecting and self-supporting. The erection of the structure takes place from the stored potential energy within the compressed composite wall. Basically, the composite consists of flexible facings and a foam core. The structure is packaged into a small volume by alternately folding and compressing the composite wall section. Upon release of the constrained structure in space, the stored potential energy is sufficient to erect the structure and allow it to be self-supporting without any external influences.

This concept was initially investigated by Narmco under Contract NASw-661, entitled "Development and Evaluation of the Elastic Recovery Concept for Expandable Space Structures" (Reference 1). This study resulted in the determination of the possible areas of application for the elastic recovery principle.

The present contract was a continuation effort whose objective was to determine the feasibility of designing an expandable airlock utilizing elastic recovery materials. The parameters investigated included micro-meteoroid and thermal protection, maximum flexibility, multiple deployment – retraction cycles, and minimum leakage. The design of the expandable airlock is shown in Figure 1.

The subsequent text delineates the methods and approach used in the determination of these requirements.

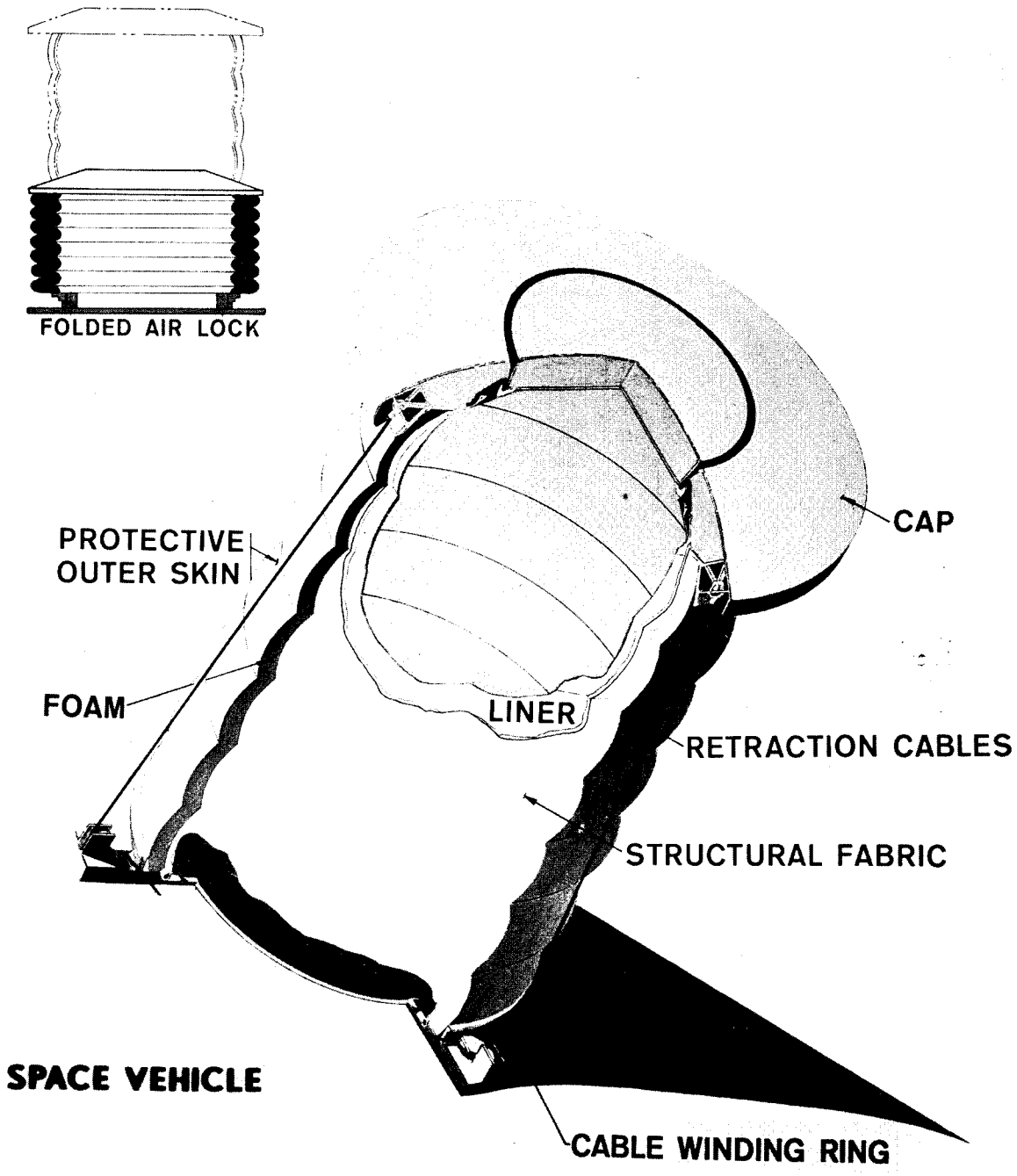

Figure 1. Expandable Airlock

II. DESIGN CRITERIA

The basic design criteria or guidelines for the development of the expandable airlock are listed in Table 1.

The primary requirement was to design an airlock which provides protection from the space environment and still maintains the necessary flexibility for packaging. An additional requirement was that the airlock system have the capability of being repackaged during the mission.

TABLE 1

DESIGN CRITERIA FOR THE EXPANDABLE AIRLOCK

Orbit Parameters	200-nm circular orbit 28.7° inclination
Internal Temp Range	50°-80°F with a design temp of 64°F
Thermal Control	Passive system only Reflection from a space station to be considered as that from a 260-in. dia, circular, flat section
Structural Design	Internal pressure to 10 psi operating Burst (ult.) factor safety = 5
Hatch Design	Opening force of 40 lb or less with no pressure differential Capability of being opened from either side
Leakage	Max. of 0.01 lb/day @ 1-atm pressure differential & 60°F temp
Meteoroid Protection	Critical meteoroid mass used for the analysis & the test results discussed in Section VI
Radiation	Not designed into the airlock wall due to the short periods of time the astronaut is in the airlock (see Section VII)

III. MATERIALS

The materials for the expandable airlock wall were divided into four major functional categories: the outer thermal control surface, layers for meteoroid and thermal protection, structural fabric, and inner impervious layer. (The layers for the environmental protection also provide the elastic recovery mechanism for airlock deployment.)

A. Thermal Control Surface

The thermal control surface was not, as such, determined during this expandable airlock feasibility study. However, through the thermal analysis (Section IV), the required surface characteristics for the solar absorptivity and emissivity were found to be $\alpha_s = 0.19$ and $\epsilon = 0.25$, respectively. These optical values will maintain the internal air temperature of the airlock within the required range when subjected to maximal heating.

The second thermal condition, minimal heating, causes the temperature to stabilize at a level below the design limits. However, this range is within the temperature capabilities of the elastic recovery materials.

It is anticipated that the coating which gives the required optical properties will be determined by test during the next phase of work. Some of the tests will be performed on cloth which has direct application of the thermal control coating by electro-chemical deposition.

This technique has been investigated by Narmco and appears to be feasible. If optical properties can be achieved by this approach, an improvement in composite flexibility could be obtained.

B. Materials for Micrometeoroid Protection

The materials for micrometeoroid protection consist of flexible laminate bumper layers and polyurethane foam.

The latter type of material serves three functions by (1) providing the elastic recovery mechanism, (2) providing thermal insulative qualities, and (3) absorbing the fragments of the micrometeoroid particle. The type of foam used in the study was open cell of approximately 1.3-lb/ft^3 density. This type of foam was found, from previous experience, to be best suited for the elastic recovery mechanism (Reference 1). Lighter density foam did not have the substance for elastic recovery, and heavier foam would result in a weight penalty.

The material for the laminate layers of the composite layer evolved from the opposite requirements of thickness required for micrometeoroid fragmentation and flexibility necessary for packaging. For the laminates, four types of adhesive materials were considered as possible candidates. These materials are listed in Table 2.

TABLE 2

CANDIDATE ADHESIVE MATERIALS

Resin	Elastomer
Polyvinylidene Chloride Latex	RTV silicone rubber
Polyeythylene	
Polyurethane	

The last resin system listed, polyurethane, and also RTV silicone rubber are the preferred adhesive materials since with these materials elevated temperature is not required for curing.

During the early phases of the program, the polyvinylidene chloride resin looked most promising from experience gained in fabricating flat sample panels. However, processing difficulties occurred when the resin was used for fabricating a large-size panel. The problems resulted from the high viscosity of the resin and the 250°F temperature required for cure. For large area bonds, the combination of time and temperature degraded both the foam and resin.

The use of polyethylene film as the matrix and adhesive for bonding cloth to foam was also evaluated. A temperature of approximately 220°F was required to fuse the film to the cloth and the foam. The result was an adequate-strength bond and improved flexibility. This technique of bonding the cloth to foam with a film material was not attempted on a large surface panel; hence, the time and temperature effects were not determined. Use of the polyethylene film resulted in flexible composite sections due to the fact that there was limited impregnation of the film into the cloth or foam.

The technique for limiting the resin impregnation was found to be the key to improved composite flexibility. Several methods for limiting the impregnation were attempted by Narmco; these included changing the resin viscosity and utilizing different methods of application.

The primary method used to change the resin characteristic was by the addition of thickeners. The polyvinylidene chloride latex was the only resin system on which this approach was attempted because of its high viscosity. The thickener recommended for this system by the supplier was hydroxyethyl cellulose. This material improved the polyvinylene chloride so that it did not soak into the foam or cloth. However, a curing temperature was still required, which made this material less desirable than a room temperature curing resin.

The second method for improving laminate flexibility (limiting the resin impregnation) was used primarily on the room temperature curing systems. Several methods of limiting the impregnation of the cloth or foam were

available for use, which included application of the resin by brushing, spraying, or transferring. Experiments on flat panels showed that the brushing and spraying methods resulted in too heavy a resin application for maximal flexibility. Additionally, there was difficulty in maintaining a uniform coating of resin on either cloth or the foam. Brushing the resin on the foam was especially difficult due to the latter's compliance.

The third method of limiting resin impregnation (transferring) was found by Narmco to be the most effective means to achieve maximal flexibility. The transfer method is a two-step procedure, whereby the resin is first spread out in a film, and then allowed to advance to a B-stage of tackiness. The cloth or foam is then laid on the resin to pick up enough to cover the surface. The materials are then bonded together with contact pressure. An example of composite flexibility obtained by this technique is shown in Figure 2. The cloth and foam layers represent the thickness required for meteoroid protection.

Regenerated cellulose fiber cloth was used throughout this investigation. Based on samples of the different fabrics available, including those of polyester fiber, the former exhibited better drape qualities, which could be indicative of the flexibility. The cloth used for the micrometeoroid bumper does not require high strength as such, since the phenomenon of hypervelocity impact probably does not apply a steady-state loading condition to the fabric. This suggests that bumper cloth material substitution can be made without changing the effectiveness of the micrometeoroid protective system.

C. Selection of Filamentary Material

In reviewing requirements for the airlock wall, a survey of available filamentary materials limited consideration to a few materials. These selections are listed in Table 3, together with mechanical properties. Of these materials, the polyester filaments have the best combination of properties.

Based on available data, as well as on extensive experience at Astro Research Corporation (subcontracted by Narmco) in the use of filamentary materials as load-carrying elements in various types of structures, high-tenacity Dacron polyester filaments have been selected for the load-carrying structure. This material has a high, quick-breaking tenacity; low growth under load; a superior creep-rupture characteristic; is less affected by gamma-radiation than nylon, has a high ability to endure large, permanent deformation without rupture. In the working range, Dacron has a nearly linear stress-strain curve, in contrast to an irregular curve for Fortrel polyester fiber, and also has a higher modulus of elasticity than the latter. For these reasons, Dacron is the preferred material.

D. Liner Material

The purpose of the inner liner was to retain the air within the airlock. The desired material properties were flexibility, toughness, and low

(a) Folded

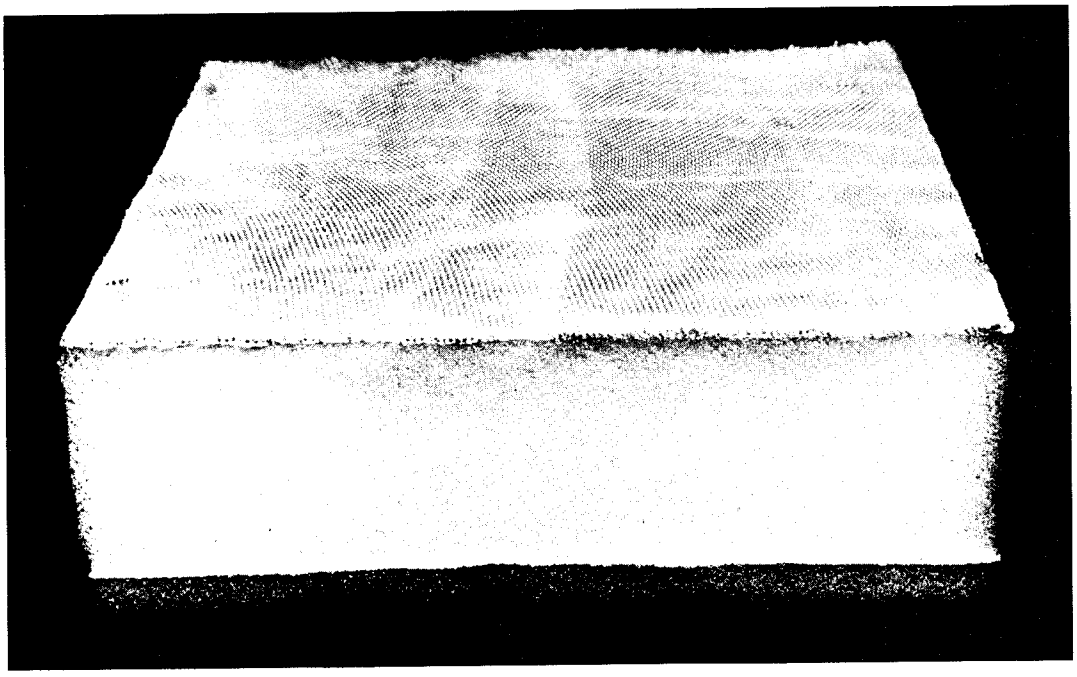

(b) Unfolded

Figure 2. Flexible Elastic Recovery Materials

TABLE 3

MECHANICAL PROPERTIES OF FILAMENTS*

Property	Polyester		Nylon	Rayon	
	Dacron (High-Tenacity Filament)	Fortrel (High-Tenacity Filament)	Nylon 6,6 (High-Tenacity Filament)	Avril (Staple)	Fortisan (Filament)
Ult. Tensile Strength, psi	140,000	140,000	134,000	100,000	136,000
Breaking Elongation, %	10 - 13	8 - 10	16 - 28	18	6
Elastic Recovery, %	100 @ 1%	100 @ 2%	100 @ 4%	--	100 @ 20%
Specific Gravity	1.38	1.38	1.14	1.5	1.5
Specific Strength, x 10^6 in.	2.8	2.8	3.2	1.8	2.5
Effect of Heat	Sticks @ 445°F; m.p. 482°F	m.p. 485°-510°F	m.p. 480°F	Decomposes @ 350°-400°F	Decomposes @ 360°F

* Data taken from Reference 7

permeability. A review of candidate film materials showed polyvinylidene chloride film has the lowest permeability. The comparison of this material with several other films is shown in Table 4.

The thickness of the film required to prevent extrusion through the structural fabric was determined by test. A simple frame was constructed to simulate, as closely as possible, the actual loading condition upon the film material. The frame held a sample of the structural fabric against which a piece of the film was placed for testing. The frame fixture was closed and air used to pressurize the cavity between the film and fixture back. Since the fabric was designed to burst at 50 psi, the maximum pressure used for the test was 45 psi. The test fixture is shown in Figure 3 during a test.

The result of the test indicated that a 3/4-mil thickness of polyvinylidene chloride film would not extrude through the structural fabric mesh when under the maximum test pressure of 45 psi. To provide an additional safety factor, the liner thickness for the airlock was arbitrarily increased to 2 mils.

TABLE 4

PERMEABILITY OF FILM MATERIALS*

Material	Permeability to Gases, $\frac{\text{cc-mil}}{100\ \text{in.}^2/24\ \text{hr/atm}}$			
	Nitrogen	Oxygen	Carbon Dioxide	Water Vapor @ 100% Humidity
Polyvinylidene chloride (Saran)	0.86	3.0	9.0	11.5
Polyester terephthalate (Mylar)	1.2	5.6	27	1485
Polyvinyl chloride (PCV)	43	123	58	-
Polytetrafluoroethylene	9.5	30	-	-
H-Film	5.8	24.5	-	-
Polyethylene	210	655	2240	

* Data taken from the compilation in Reference 1

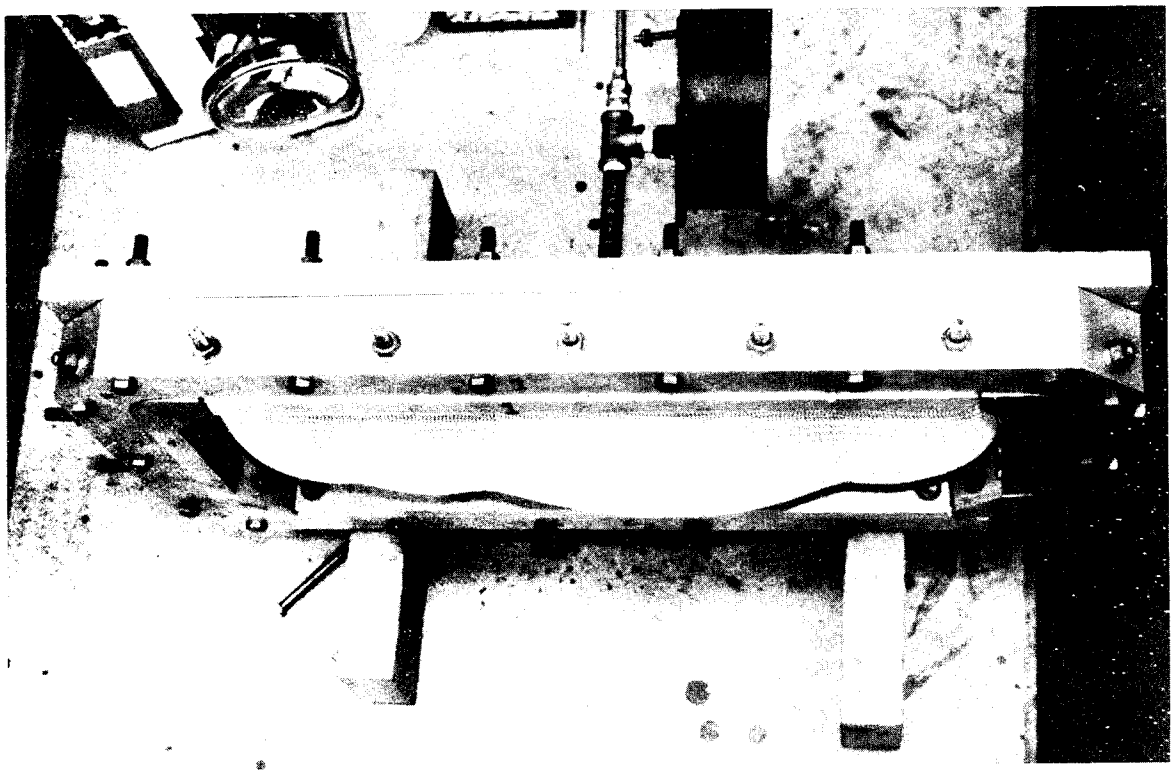

NOTE: The knitted structural fabric is visible in this figure. The liner serves as the bladder.

Figure 3. Liner Test Fixture

IV. EXPANDABLE AIRLOCK THERMAL ANALYSIS

This section of the report presents the thermal design study for the expandable airlock. The temperature history of the cylindrical airlock structure and the internal air mass were determined.

The method of analysis utilized a computer program which determined the effectiveness of various α_s/ϵ_t optical coatings and thickness of foam insulation for control of the internal air temperature. The airlock operating environment was assumed to be a 200-nm orbit at an inclination angle of 28.7 degrees. The analysis considered both maximal and minimal sun exposure.

For the maximal heating condition, an airlock wall with optical surface properties of $\alpha_s = 0.19$ and $\epsilon_t = 0.25$ and also 2 in. of foam maintained the internal temperature within the specified limits. This composite construction also performed satisfactorily at the minimal heating condition, although the internal temperature stabilized at -40°F after several orbits.

A. Nomenclature

The following list defines the symbols used in this analysis:

A	Surface area, ft^2
c_p	Specific heat, Btu/lb °F
D	Diameter of cylinder, ft
E	Earth-emitted radiation flux, Btu/hr ft^2
F	Form factor
H	Height of cylinder, ft
h	Convective heat transfer coefficient, Btu/hr ft^2 °F
I	Irradiation heat flux, Btu/hr ft^2
k	Coefficient of thermal conductivity, Btu/hr ft °F
L	Diagonal of rectangle enclosing cylinder, ft
L_B	Total radiation heat flux leaving a surface, Btu/hr ft^2
P	Air pressure, psia
q	Heat flow rate, Btu/hr
R	Radius, ft
r	Radial coordinate, ft
r_E	Earth's planetary albedo
S	Solar constant, Btu/hr ft^2
T	Temperature, °F or °R
t	Time, hr
W	Mass, lb

X	Rectangular coordinate, ft
Y	Rectangular coordinate, ft
Z	Vertical coordinate, ft
α	Absorptivity
β	Cylindrical coordinate, degrees
ϵ	Emissivity
ℓ	Distance between differential areas, ft
ρ	Reflectivity
σ	Stefan-Boltzmann constant, Btu/hr ft^2 R^4
ϕ	Angle from surface normal, degrees
θ	Angle of airlock diagonal from base

Subscripts:

A	Air
B	Base plate
C	Cylinder
E	Earth
e	External
i	Internal
R	Albedo (Form Factor)
s	Solar
T	Thermal

B. Discussion

The use of composite structural materials such as reinforced plastic skins and polyurethane sandwich core presents very definite temperature limitations on the vehicle. The maximal allowable temperature of the foam material in a space vacuum environment is approximately 250°F. Above this temperature, the foam will lose its elastic recovery characteristics and above 300°F it will lose its structural integrity.

For this reason, temperature control of the airlock structure becomes a primary design criterion. The requirement of maintaining a shirt-sleeve, 64°±15°F environment in the interior of the airlock further necessitates an extensive and accurate thermal analysis.

The thermal environment of an orbiting vehicle is established by radiation heat influx on the external surfaces. In a low earth orbit, the solar radiation, albedo, and earth-emitted thermal radiation are the contributing factors of the total heat influx. In the case of an airlock structure which is not an independent vehicle in orbit but is attached to a larger spacecraft, the effect of reflected and emitted radiation from the surfaces of the space vehicle must be included in the thermal analysis.

The radiation thermal environment varies greatly from point to point around the orbit and is dependent on the relative magnitude of sun exposure and shadow periods, besides being a function of the vehicle orientation relative to the orbit plane.

The complexity of an accurate analysis of the thermal environment as influenced by all of these variables suggested the use of computer solution.

Computer programs are available which determine the radiation heat influx on the external surfaces of simple geometry vehicles in earth orbit. A North American Aviation, Inc. developed computer program determines radiation form factors of a multisurfaced space vehicle for solar, albedo, and earth-emitted radiation incident upon each vehicle surface at various intervals around the orbit. This program is also capable of evaluating the transient heat balance for each external surface of the vehicle, computing the temperature of the individual surfaces at a large number of points around the orbit.

The North American computer program was selected for use in the thermal analysis of the expandable airlock. However, extensive modification of this program was required in order to allow its use as an effective design tool in determining the optimal insulation thickness and spectral surface coating properties for the expandable airlock.

The modified program determined the net radiation heat flux caused by direct solar, earth reflected solar, and earth thermal radiation for each flat surface segment of the vehicle at a large number of steps around the orbit. The external heat balance computation also included reflected solar radiation from a large base plate combined with thermal radiation from this plate at a constant, predetermined emitting temperature. Furthermore, the program evaluated the transient, one-dimensional heat transfer rates across the composite insulated wall of the vehicle for a large number of increments between each computation step of the external radiation heat transfer. At each interval, the temperature of the external and internal wall surfaces and the average temperature of the internal air mass were determined.

C. Critical Design Conditions

An orbit altitude of 200 nm and an inclination angle of the orbit plane of 28.7 degrees were specified for the airlock's particular mission. However, the date of the mission and its duration, and spacecraft and airlock orientation relative to the earth or sun position, were not specified. Under these conditions, a large number of thermal environments could be investigated. In order to demonstrate the feasibility of the expandable airlock concept from the thermal viewpoint, the two extremes of the environmental spectrum were selected as critical design conditions: these are the maximal and minimal heating conditions.

1. Maximal Heating Environment

The relative duration of sun exposure and shadow periods for a given altitude and inclination orbit change during the year. The maximal

sun exposure period will occur when the angle between the solar radiation and the orbit plane is at its maximal value.

The total solar radiation heat influx on the vehicle is also the function of the orientation of the cylindrical airlock and the large spacecraft to which it is attached. The critical orientation for maximal heating of the cylindrical airlock was determined.

2. Minimal Heating Environment

The most severe cold environmental condition for the airlock will occur when it receives the minimal amount of heating from the sun. The shadow period is longest when the sun is in the orbit plane of the vehicle during the vernal or autumnal equinox.

Vehicle orientation resulting in minimal sun exposure is one where the airlock is in the shadow of the space vehicle throughout the orbit.

D. Radiation Heat Exchange between the Airlock and the Space Vehicle

The effect of the large space vehicle on the thermal environment of the airlock was simulated by the radiation heat exchange between the airlock and an approximate 260-in. diameter, circular base plate. The airlock was assumed to be located in the center of the base plate.

Computation of net radiant heat exchange between the cylindrical airlock and a circular base plate was extremely complex for this general case, which involved thermal radiation from the vehicle surfaces, and reflected solar and albedo radiation which were considered with changing shadow geometries around the orbit. However, by assuming a fixed vehicle orientation throughout the orbit, and by neglecting the effect of airlock's shadow on the base plate, an analytical expression was derived for the radiation heat exchange:

Assumptions:

a. The reflected radiation from the base plate is diffused and follows Lambert's Law.

b. The circular base plate is isothermal.

c. No shadow is formed on the base plate by the airlock.

d. Earth thermal radiation and earth-reflected solar radiation reflection from the base plate are negligible.

e. Secondary reflection between the airlock and the cylinder is negligible.

Let $I_{B(s)}$ be the total solar irradiation per unit area on the circular base plate.

The solar reflection from a differential area dA_B of the base plate is $\rho_s I_{B(s)}$, where $\rho_s = 1 - \alpha_s$.

The total radiation leaving a differential area dA_B of the base plate $\left(L_B dA_B\right)$ is equal to the sum of reflected solar radiation and emitted thermal radiation (Reference 2).

$$L_B dA_B = \left(\rho_s I_{B(s)} + \epsilon_T \sigma T_B^4\right) dA_B$$

The incident radiant flux received by a differential element dA_C on the cylindrical surface from a differential area dA_B of the circular base plate $I_{C(dA_B)}$ is equal:

$$I_{C\left(dA_B\right)} = \frac{L_B \, dA_B \cos \phi_B \cos \phi_C}{\pi \ell^2}$$

$$I_{C\left(dA_B\right)} = L_B \, F_{dA_B} \, dA_C$$

where $F_{dA_B dA_C}$ is the geometric form factor between dA_B and dA_C.

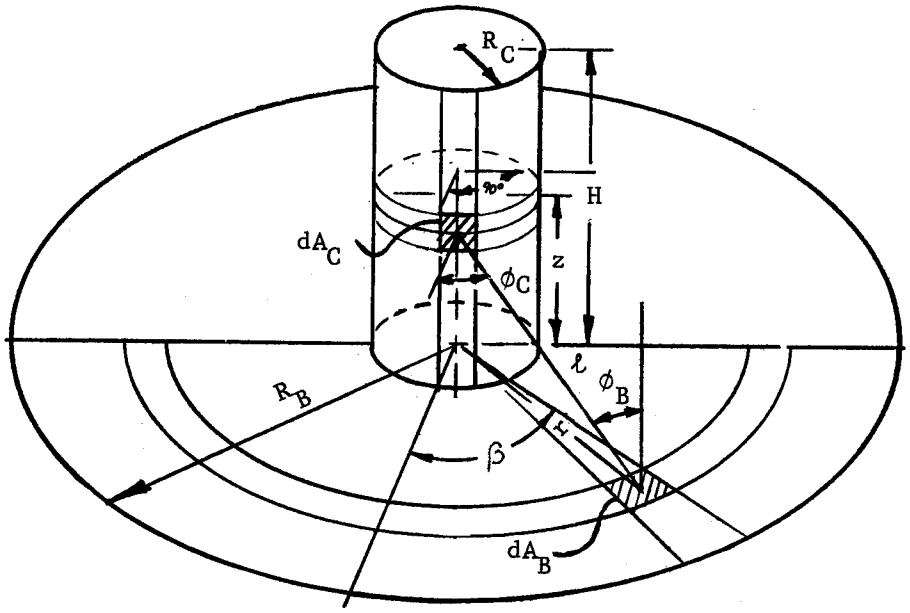

Figure 4. Form Factor Notation

Based on assumption b, L_B is constant over the base plate. The average incident radiation heat flux received by the cylinder from the base plate is equal to the product of total geometric form factor and $I_C\left(dA_B\right)$

$$\bar{I}_{C(B)} = L_B F_{B\to C}$$

The geometric form factor was computed from Lambert's Law (Reference 3):

$$F_{B\to C} = \frac{1}{A_C}\int_{A_C}\int_{A_B} \frac{\cos\phi_C \cos\phi_B \, dA_B \, dA_C}{\pi \ell^2}$$

From Figure 4,

$$\cos\phi_C = \frac{r - R_C}{\ell}$$

$$\cos\phi_B = \frac{Z}{\ell}$$

$$\ell = \sqrt{r^2 - 2R_C r \sin\beta + R_C{}^2 + Z^2}$$

$$F_{B\to C} = \frac{1}{A_C}\int_{A_C}\int_{A_B} \frac{\left|r - R_C\right| (Z)(r) \, d\beta \, dr \, dA_C}{\pi\left(r^2 - 2R_C r \sin\beta + R_C{}^2 + Z^2\right)^2}$$

$$= \frac{1}{A_C}\int_{A_C}\left[\int_{R_C}^{R_B}\int_{o}^{\sin^{-1}\frac{R_C}{R_B}} \frac{Z\left(r^2 - rR_C\right) d\beta \, dr}{\pi\left[\left(r^2 + R_C{}^2 + Z^2\right) - 2R_C r \sin\beta\right]^2}\right] dA_C$$

Closed form integration of this equation was not completed, since evaluating the geometric form factor in closed form is difficult; therefore, the form factor was rewritten in finite difference form.

The base plate surface is divided into unit areas ΔA_{Bi} . A flat strip (1-ft width) on the surface of the cylinder is divided into small areas ΔA_{Ci} , as shown in Figure 5.

The finite difference form factor equation is given below:

$$F_{B\to C} = \frac{2}{A_C} \sum_{j=1}^{m} \Delta A_{Cj} \sum_{i=1}^{n} \frac{\cos \phi_{Cj} \cos \phi_{Bi} \Delta A_{Bi}}{\pi \ell_{ij}^2}$$

This equation gives the total form factor between a flat vertical strip of the cylinder wall and the portion of the circular base plate visible from the flat strip.

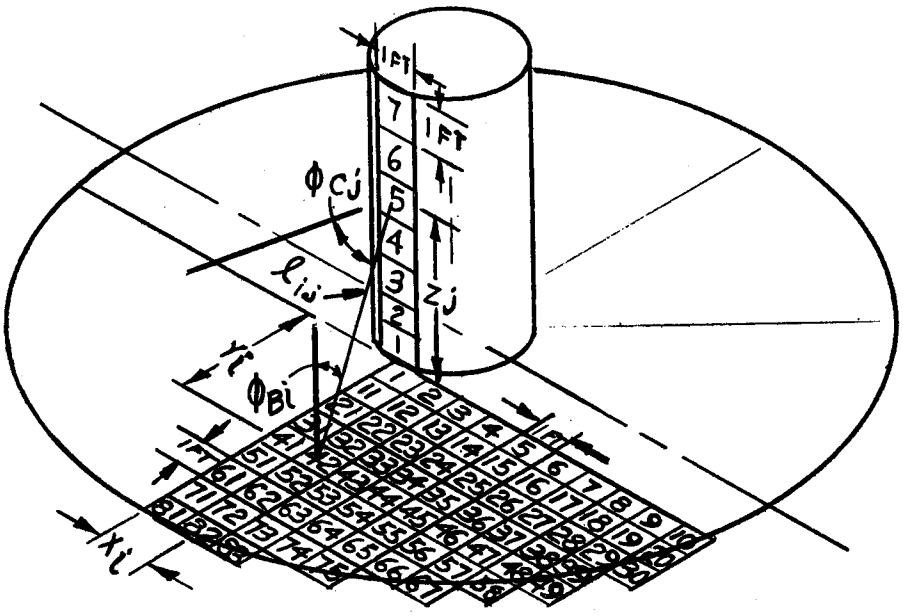

Figure 5. Finite Difference Form Factor Notation

From Figure 5,

$$\cos \phi_{Cj} = \frac{Y_i}{\ell_{ij}} \qquad \ell_{ij} = \sqrt{Z_j^2 + Y_i^2 + X_i^2}$$

$$\cos \phi_{Bi} = \frac{Z_j}{\ell_{ij}} \qquad \Delta A_{Bi} = 1 \text{ ft}^2$$

$$\Delta A_{Cj} = 1 \text{ ft}^2$$

$$F_{B\to C} = \frac{1}{7}\left[F_{B\to C_1} + F_{B\to C_2} + F_{B\to C_3} + F_{B\to C_4} + F_{B\to C_5} + F_{B\to C_6} + F_{B\to C_7}\right]$$

$$F_{B\to C_1} = \frac{2}{\pi}\sum_{i=1}^{83} \frac{0.50\ Y_i}{\left(0.25 + Y_i^2 + X_i^2\right)^2} = 0.4866$$

$$F_{B\to C_2} = \frac{2}{\pi}\sum_{i=1}^{83} \frac{1.50\ Y_i}{\left(2.25 + Y_i^2 + X_i^2\right)^2} = 0.4069$$

$$F_{B\to C_3} = \frac{2}{\pi}\sum_{i=1}^{83} \frac{2.50\ Y_i}{\left(6.25 + Y_i^2 + X_i^2\right)^2} = 0.3378$$

$$F_{B\to C_4} = \frac{2}{\pi}\sum_{i=1}^{83} \frac{3.50\ Y_i}{\left(12.25 + Y_i^2 + X_i^2\right)^2} = 0.2795$$

$$F_{B\to C_5} = \frac{2}{\pi}\sum_{i=1}^{83} \frac{4.50\ Y_i}{\left(20.25 + Y_i^2 + X_i^2\right)^2} = 0.2299$$

$$F_{B\to C_6} = \frac{2}{\pi}\sum_{i=1}^{83} \frac{5.50\ Y_i}{\left(30.25 + Y_i^2 + X_i^2\right)^2} = 0.1882$$

$$F_{B\to C_7} = \frac{2}{\pi}\sum_{i=1}^{83} \frac{6.50\ Y_i}{\left(42.25 + Y_i^2 + X_i^2\right)^2} = 0.1547$$

$$\therefore F_{B\to C} = 0.2977$$

The above equations were computed on a small Clary electronic computer. Having computed the total form factor between the base plate and a vertical strip of

the cylinder, the radiant heat influx from the base plate to a unit area of the cylinder surface is

$$I_{C(B)} = F_{B\to C}\left[\rho_s F_s S + \epsilon_T \sigma T^4\right]_B$$

E. Vehicle Orientation for Maximal Heating

Assumptions:

a. The base plate radiates at a constant temperature independent of orientation.

b. The total thermal and reflected solar radiation received by the airlock from the earth's surface is independent of orientation.

Based on the noted assumptions, only the direct solar radiation and the base reflected solar radiation are the functions of the vehicle orientation.

From Lambert's Law, the direct solar radiation received by the cylinder is equal to the solar constant times the projected cylinder area on a plane perpendicular to the sun vector.

$$I_{\substack{\text{cylinder}\\(\text{direct solar})}} = S\, A_{\substack{\text{projected}\\\text{cylinder}}}$$

From the preceding section, the solar radiation reflected from the base plate to the cylinder is

$$I_{\substack{\text{cylinder}\\(\text{base reflected}\\\text{solar})}} = S\, F_{B\to C}\left(\rho_s F_s\right)_B A_B$$

The total solar radiation received by the cylinder is the sum of the direct and reflected radiation.

$$I_{\substack{\text{cylinder}\\(\text{total solar})}} = S\left[A_{\substack{\text{cylinder}\\\text{projected}}} + F_{B\to C}\left(\rho_s F_s\right)_B A_B\right]$$

In this equation, the projected area of the cylinder and the solar form factor of the base plate are the only variables and are functions of the vehicle orientation.

Writing an analytical expression for the projected area of the cylinder is difficult. For mathematical simplicity, the projected area of a cube enclosing the cylinder will be used in the following analysis. Figure 6 shows the small difference in projected area of the cylinder and the enclosing cube.

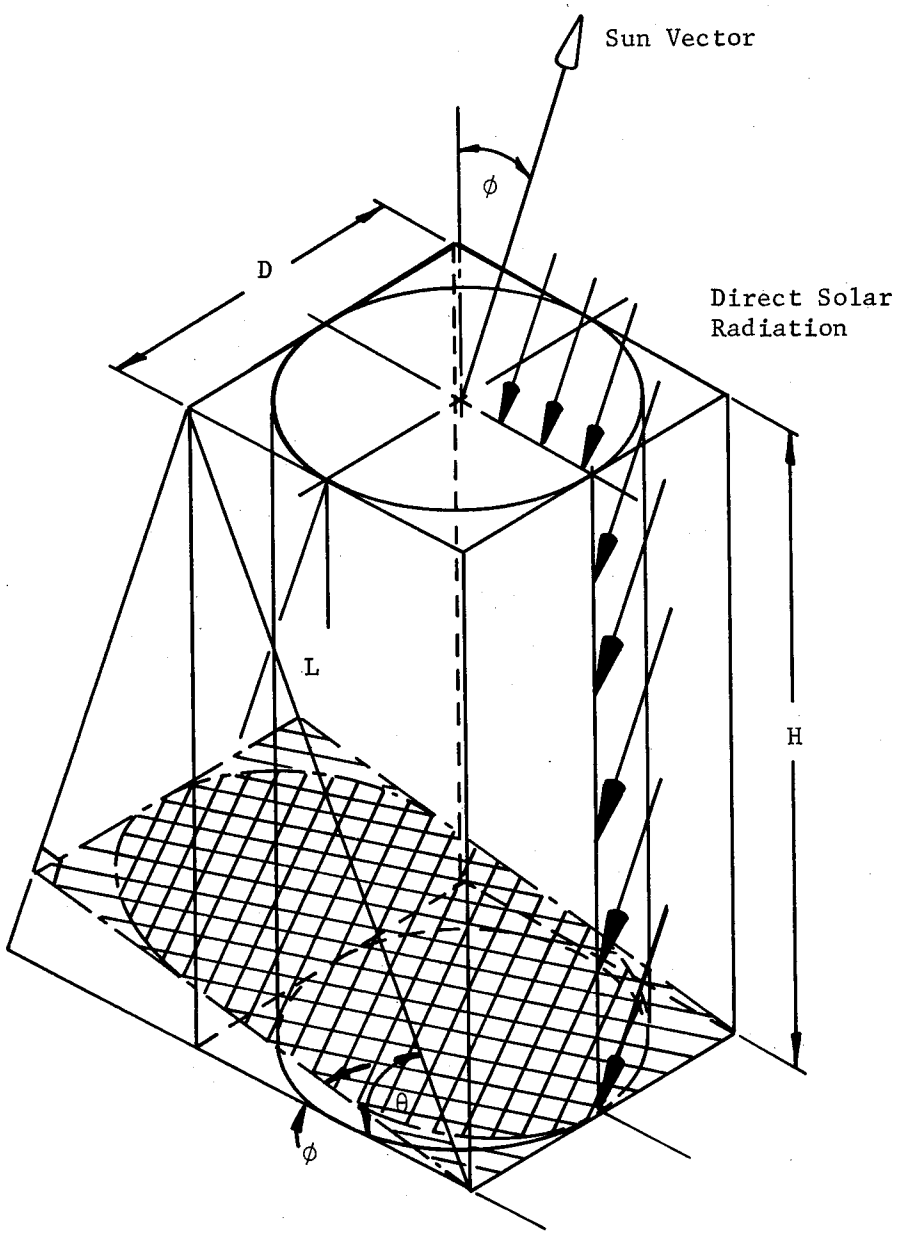

Figure 6. Projected Area Geometry

From Figure 6,

$$A_{projected} = DL \cos(\theta - \phi)$$

$$= DL (\cos\theta \cos\phi + \sin\theta \sin\phi)$$

From the geometry shown in Figure 6,

$$L = \sqrt{D^2 + H^2} \qquad \sin\theta = \frac{H}{L} = \frac{H}{\sqrt{D^2 + H^2}}$$

$$\cos\theta = \frac{D}{L} = \frac{D}{\sqrt{D^2 + H^2}}$$

Substituting into the projected area equation

$$A_{projected} = D\sqrt{D^2 + H^2}\left[\frac{D}{\sqrt{D^2 + H^2}}\cos\phi + \frac{H}{\sqrt{D^2 + H^2}}\sin\phi\right]$$

$$A_{projected} = D^2 \cos\phi + DH \sin\phi$$

The solar form factor of the base plate, $F_s = \cos\phi$ from Lambert's Law.

Substituting the approximate projected cylinder area and the solar form factor of the base plate into the equation of the total received solar radiation

$$I_{cylinder} = S\left[D^2 \cos\phi + DH \sin\phi + F_{B\to C}\,\rho_s\,A_B \cos\phi\right]$$

To find ϕ of maximal heating, $I_{cylinder}$ is differentiated with respect to ϕ total

$$\frac{dI}{d\phi} = S\left[-D^2 \sin\phi + DH \cos\phi - F_{B\to C}\,\rho_s\,A_B \sin\phi\right]$$

To maximize I_C, let $\frac{dI}{d\phi} = 0$

$$DH \cos \phi - D^2 \sin \phi - F_{B \to C} \rho_s A_B \sin \phi = 0$$

$$\tan \phi = \frac{DH}{D^2 + F_{B \to C} \rho_s A_B}$$

where for this design,

$D = 4$ ft

$H = 7$ ft

$A_B = 132$ ft^2 - Section of base plate visible from any point on the cylinder surface.

$\rho_s = 0.81$ - Assume that the base plate (space vehicle) is coated with paint similar to HAC white ($\alpha_s = 0.19$, $\epsilon = 0.93$) (Reference 2)

$F_{B \to C} = 0.2977$

$$\tan \phi = \frac{4 \times 7}{(4)^2 + (0.2977)\ (0.81)\ (132)} = 0.58541$$

$$\underline{\underline{\phi = 30^\circ\ 21'}}$$

F. Thermal Balance and Temperature Determination

In the previous sections, the critical orbit and vehicle orientation were determined for maximal and minimal heating conditions.

North American's computer program "Program for Determining the Thermal Environment and Temperature History of Orbiting Space Vehicles" (SID62-313) was utilized for both of these conditions to compute temperatures of the airlock surfaces and internal air mass at various points around the orbit.

In order to compute radiation form factors between the orbiting vehicle and the radiation sources such as the sun and the earth, the vehicle is assumed to have a number of flat, isothermal surfaces. The cylindrical airlock is analyzed as an octagonal body (shown in Figure 7) having nine external surfaces on which radiation heat transfer takes place; the bottom surface in contact with the space vehicle is assumed to be a non-heat-transferable surface.

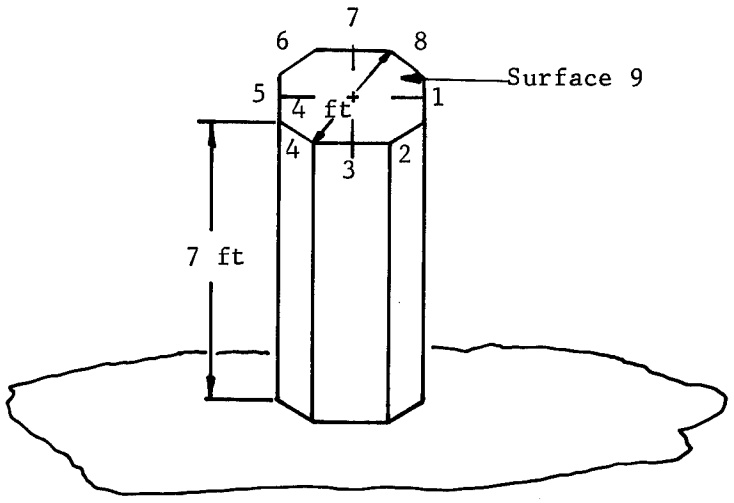

Figure 7. Octagonal Model of Airlock

The basic heat balance equation used in the North American program in its original form gave an expression for the vehicle surface temperature as a function of the incident solar, albedo, and earth-emitted radiation and also as a function of the thermal properties of the vehicle surface; i.e., solar absorptivity, thermal emissivity, specific heat, and mass. Internal heat loads on the surface were included in the computation.

$$q_{solar} + q_{albedo} + q_{earth} + q_{\substack{base \\ plate}} + q_{internal} - q_{emitted} = Wc_p \frac{dT_{surface}}{dt}$$

1. Solar Irradiation Heat Flux - q_{solar}

The solar constant in a low earth orbit is

$$S = 440 \text{ Btu/hr - ft}^2$$

The solar irradiation heat flux received by a flat surface is

$$q_{solar} = S F_s A \alpha_s$$

The solar irradiation is computed only for the maximal heating orientation of the vehicle; in the minimal heating condition, q_{solar} is zero. The maximal heating orientation was determined in the previous section as $\phi = 30°21'$, where ϕ is the angle

between the longitudinal axis of the cylinder and the sun vector. For the critical surface temperature design condition, it is assumed that the same surface remains sun-oriented throughout the orbit.

The solar radiation form factor is computed for each of the nine surfaces of the octagonal vehicle by the computer program for the specified orientation.

2. Albedo Irradiation Heat Flux - q_{albedo}

The planetary albedo for the earth is taken as $r_E = 0.34$. The albedo irradiation heat flux received by a flat surface is

$$q_{albedo} = r_E \, S \, F_R \, A \, \alpha_s$$

The albedo radiation form factor was computed by the computer program for the specified vehicle orientation.

3. Earth-Emitted Irradiation Heat Flux - q_{earth}

The earth is assumed to radiate as a gray body at a uniform temperature. The earth-emitted radiation constant is assumed to be

$$E_E = \frac{1 - r_E}{4} S = \frac{1 - 0.34}{4} \times 440 = 72.5 \text{ Btu/hr - ft}^2$$

The earth-emitted irradiation heat flux received by a flat surface is

$$q_{earth} = E_E \, F_E \, A \, \alpha_T$$

4. Radiation Emitted by the Vehicle Surfaces - $q_{emitted}$

The vehicle surfaces are assumed to radiate as gray bodies to an absolute zero sink:

$$q_{emitted} = \epsilon_T \, \sigma \, AT^4$$

5. Radiation Received from the Base Plate - $q_{\text{base plate}}$

The incident radiation of the cylinder surface received from the circular base plate was derived in a previous section:

$$I_{C(B)} = F_{B\to C}\left[\rho_s F_s S + \epsilon_T \sigma T^4\right]_B$$

The absorbed radiation heat flux by the cylinder surface is given by:

$$q_{\substack{\text{base}\\\text{plate}}} = F_{B\to C} A \alpha_s \left(\rho_s F_s\right)_B S + \alpha_T \sigma \epsilon_T T^4\Big)_B$$

The base plate temperature is held constant, independent of orbit position.

6. Internal Heat Flow - q_{internal}

The external heat transfer is limited to radiation; however, the external skin is in direct contact with the foam layer and conduction heat transfer must be considered through the sandwich wall (see Figure 8).

The conductive heat flow through the foam can be written as a function of the external and internal skin temperatures:

$$q_{e\to i} = \frac{k_f}{\ell} A \left(T_e - T_i\right)$$

Sign Convention: Heat flow into the vehicle is positive

$$q_{i\to A} = hA \left(T_i - T_A\right)$$

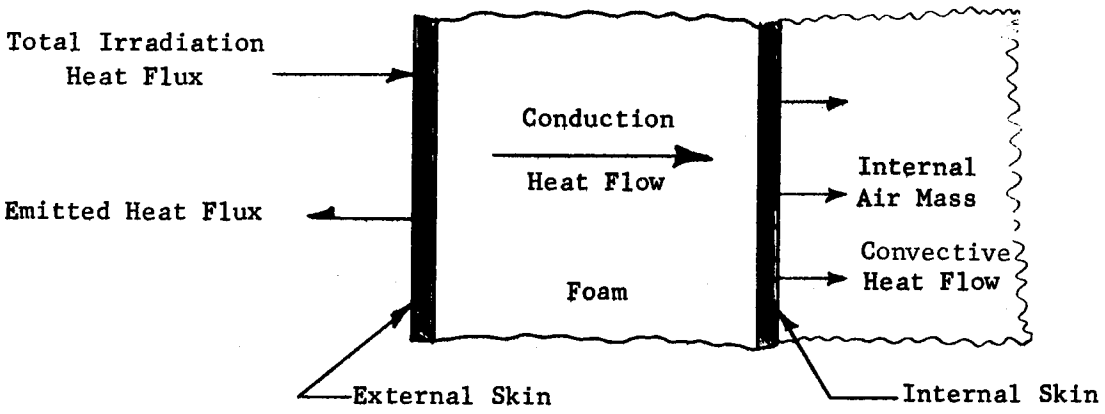

Figure 8. Heat Transfer through the Vehicle Wall

7. Summary of the Heat Balance Equations

a. External Skin

$$\alpha_s A_n F_s S + \alpha_s A_n F_E r_E S + \alpha_T A_n F_E E_E$$

$$+ A_n F_{B\to C} \left[\alpha_s \left(\rho_s F_s A \right)_B S + \alpha_T \sigma \left(\epsilon_T T^4 A \right)_B \right]$$

$$- \epsilon_T \sigma A_n T_{e_n}^4 - \frac{k_f}{\ell} A_n \left(T_e - T_i \right)_n = W_e c_{p_e} \left(\frac{\Delta T_e}{\Delta t} \right)_n$$

b. Internal Skin

$$\frac{k_f}{\ell} A_n \left(T_e - T_i \right)_n - hA_n \left(T_{i_n} - T_A \right) = W_i c_{p_i} \left(\frac{\Delta T_i}{\Delta t} \right)_n$$

c. Internal Air Mass

$$\sum_{n=1}^{9} hA_n \left(T_{i_n} - T_A \right) = W_A c_{p_A} \frac{\Delta T_A}{\Delta t}$$

G. Computer Solution

The first step in the computer solution of the finite difference heat balance equation was the evaluation of the solar, albedo, and earth-emitted radiation form factors for each surface at 5-degree intervals around the orbit.

The size of the time increments for the finite difference solution of differential equations was determined by the magnitude of the smallest thermal resistance and heat capacitance product in the system. The low value of thermal mass of the internal air determined the largest time step that could be used in the solution of the heat balance equations. However, the external radiation heat balance equation could tolerate a much larger time step. For reasons of program economy, the internal temperatures were computed 10 times for each external temperature value determined by the larger time step radiation heat balance equations.

The external and internal surface and internal air mass temperatures were computed for a minimum of three orbits for the two critical design conditions with parametric variation of surface properties and insulation thickness. Computer input data are presented in Table 5.

H. Results and Conclusions

The parametric variation of surface coating properties combined with the use of various thicknesses of foam insulations made possible the optimization of the airlock's thermal design.

The results of the computer analysis are summarized in Table 6 for the selection of surface coatings for the maximal heating condition. The temperature profiles for Coatings Nos. 5 and 6 are graphically reproduced in Figures 9 through 12.

Based on the results of the computer analysis for the maximal heating condition, a surface coating similar to Coating No. 6, with $\alpha = 0.19$ and $\epsilon_T = 0.25$, was selected.

The behavior of this design was investigated under the minimal heating condition with 2.00 and 3.00 in. of foam insulation. The results indicate that the internal air temperature drops rapidly after pressurization of the airlock at 64°F (see Figures 13 and 14). The 2.00-in. thick insulation maintains the internal air temperature within the specified limits only for 35 minutes. The increased insulation thickness does not provide enough improvement of the cooling characteristics to warrant the increased weight and volume of the 3.00-in. thick foam wall.

After several orbits, the internal air temperature stabilizes around -40°F (see Figures 15 and 16), and the lowest temperature on the external surfaces is -85°F, which has no adverse affect on the vehicle structure.

TABLE 5

COMPUTER INPUT DATA

Orbit Information			
1. 200-nm circular orbit; inclination angle, i = 28.7 degrees 2. Max. heating epoch time t_o = 21 June 1964 3. Min. heating epoch time t_o = 21 Sept 1964			
Vehicle Orientation			
1. Max. heating: Angle between sun vector & normal of surface No. 1 (see Figure 8) = 60 degrees, constant 2. Min. heating: Angle between sun vector & normal of surface No. 9 = 180 degrees, constant			
Initial Temp			
1. Initial temp of vehicle: 64°F 2. Circular base plate has a constant temp of 0°F			
Coating Properties			
Material	Solar Absorptivity	Emissivity	Reference No.
Aluminized Mylar	0.35	0.20	(4)
Teflon FEP	0.16	0.89	(2)
Alodine 401-41	0.40	0.50	(4)
White silicon - alkyde - black enamel coatings No. 3	0.40	0.92	(5)
Coating No. 5	0.17	0.20	
Coating No. 6	0.19	0.25	

TABLE 5 (Continued)

Base Plate Properties*

1. Solar absorptivity: 0.19
2. Solar reflectivity: 0.81 Reference 2
3. Thermal emissivity: 0.93

Sandwich Wall Properties

Component	Thickness, in.	Thermal Conductivity, Btu/hr ft °F	Mass, lb/ft^2	Specific Heat, Btu/lb °F
External skin	0.05	-----	0.444	0.25
Foam	1.90	0.015	0.192	----
Internal skin	0.05	-----	0.313	0.25

Internal Air Mass

1. Volume: 87.92 ft^3
2. Pressure: 10 psi
3. Density: 0.0566 lb/ft^3
4. Specific heat: 0.24 Btu/lb °F
5. Mass: 4.97 lb

Convective Heat Transfer Coefficient

$$h = 0.29 \left(\frac{P}{14.7}\right)^{\frac{1}{2}} \left(\frac{\Delta T}{H}\right)^{\frac{1}{4}}$$

Assume: $\Delta T = 50°F$

$$h = 0.29 \left(\frac{10}{14.7}\right)^{\frac{1}{2}} \left(\frac{50}{7}\right)^{\frac{1}{4}} = 0.29 \times 0.825 \times 1.64 = \underline{\underline{0.392}} \text{ Btu/hr ft}^2 \text{ °F}$$

* Assumed to have typical thermal control surface used on metal surfaces (e.g., HAC white)

NOTE: Thermophysical properties of reinforced plastic laminates and air taken from Reference 6

Thermal conductivity of polyurethane foam measured by Narmco in vacuum (10^{-4} in. Hg) at 200°F temperature

TABLE 6

SUMMARY OF COMPUTER ANALYSIS; MAXIMUM HEATING CONDITION

Coating	α_s	ϵ_t	α_s/ϵ_t	Foam Thickness, in.	Max. Surface Temp, °F	Comments
Aluminized Mylar	0.35	0.20	1.75	0.20	290	External surface temps exceed allowable temp of composite materials
Teflon FEP	0.16	0.89	0.18	0.20	18	Av. temp too cold
White Silicon-Alkyde Black Enamel	0.40	0.92	0.44	2.00	117	Av. internal air temp too cold
Alodine 401-41	0.40	0.50	0.80	0.20	190	Av. internal air temp too high. Insulation thickness is not sufficient to control internal air temp oscillation
Coating No. 5 (Figures 9 & 10)	0.17	0.20	0.85	2.00	150	Satisfactory design; internal temp variation 62°F to 49°F
Coating No. 6 (Figures 11 & 12)	0.19	0.25	0.80	2.00	185	Satisfactory design; internal temp variation 82°F to 52°F. Internal air temp range should be lowered to 79°F to 49°F

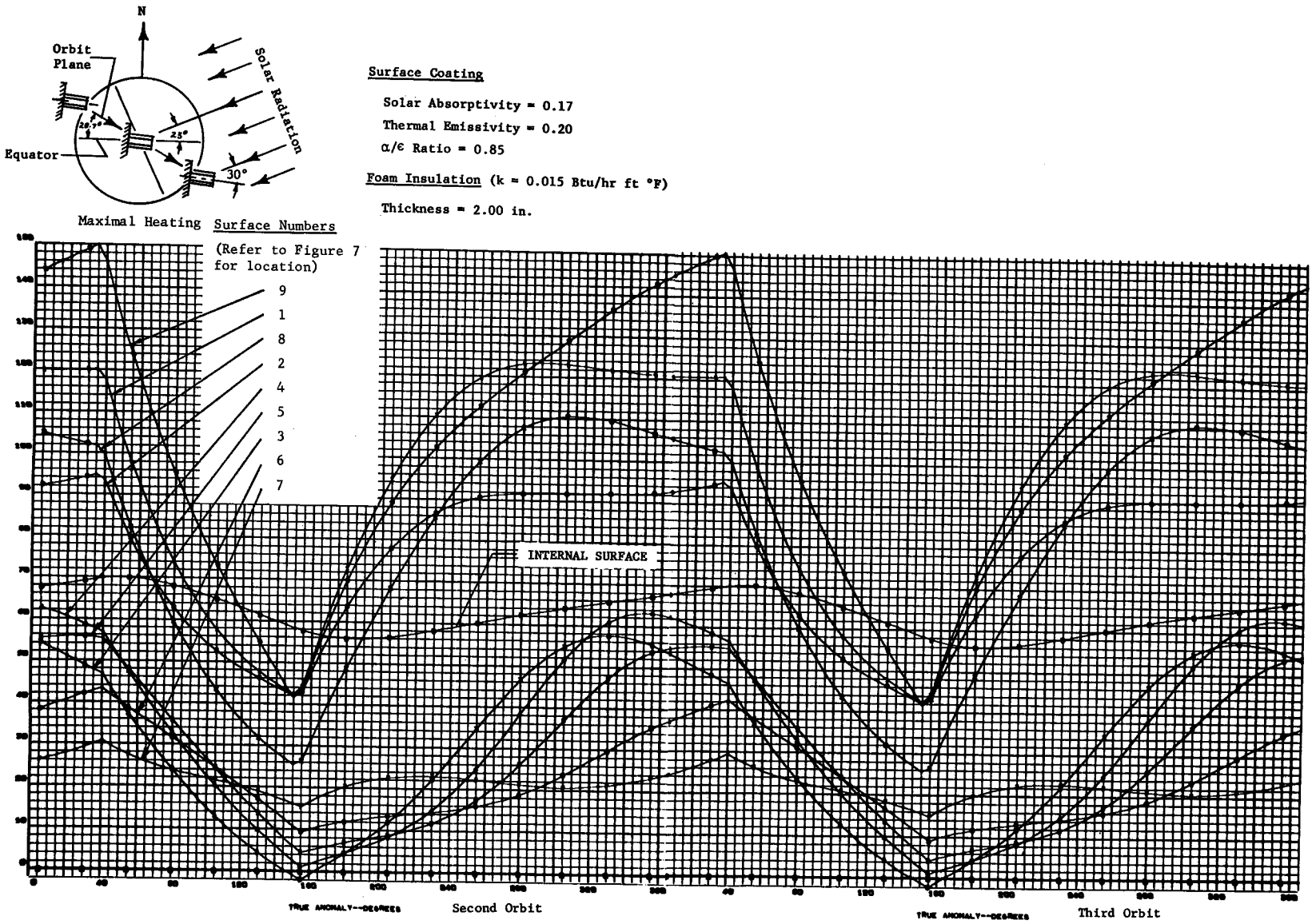

Surface Coating

Solar Absorptivity = 0.17

Thermal Emissivity = 0.20

α/ϵ Ratio = 0.85

Foam Insulation (k = 0.015 Btu/hr ft °F)

Thickness = 2.00 in.

Figure 9. External Surface Temperatures

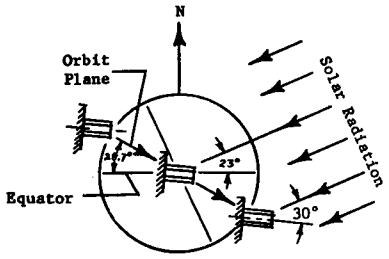

Maximal Heating

Surface Coating

Solar Absorptivity = 0.17

Thermal Emissivity = 0.20

α/ϵ Ratio = 0.85

Foam Insulation (k = 0.015 Btu/hr ft °F)

Thickness = 2.00 in.

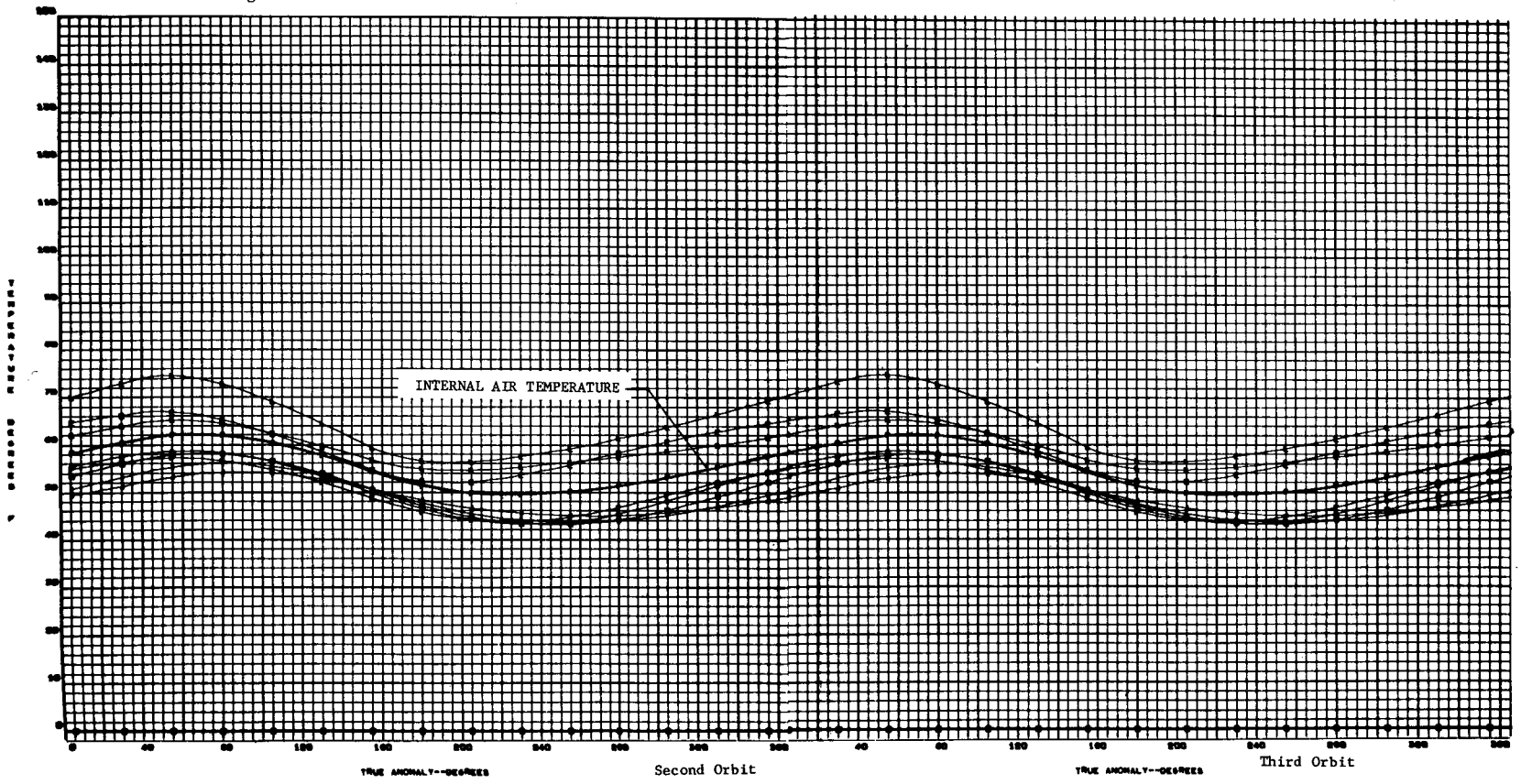

Figure 10. Internal Temperatures

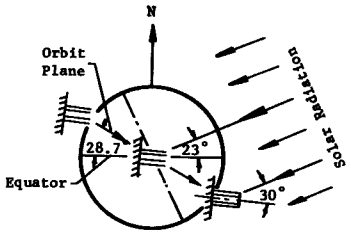

Maximal Heating

Surface Coating

Solar Absorptivity = 0.19

Thermal Emissivity = 0.25

α/ϵ Ratio = 0.80

Foam Insulation (k = 0.015 Btu/hr ft °F)

Thickness = 2.00 in.

Surface Numbers

(Refer to Figure 7 for location)

9
1
2
8
6
4
3
7
5

INTERNAL SURFACE

First Orbit

Second Orbit

Third Orbit

True Anomaly - Degrees

Figure 11. External Surface Temperature

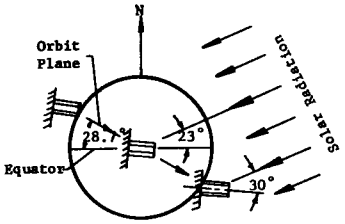

Maximal Heating

Surface Coating

Solar Absorptivity = 0.20

Thermal Emissivity = 0.25

α/ϵ Ratio = 0.80

Foam Insulation (k = 0.015 Btu/hr ft °F)

Thickness = 2.00 in.

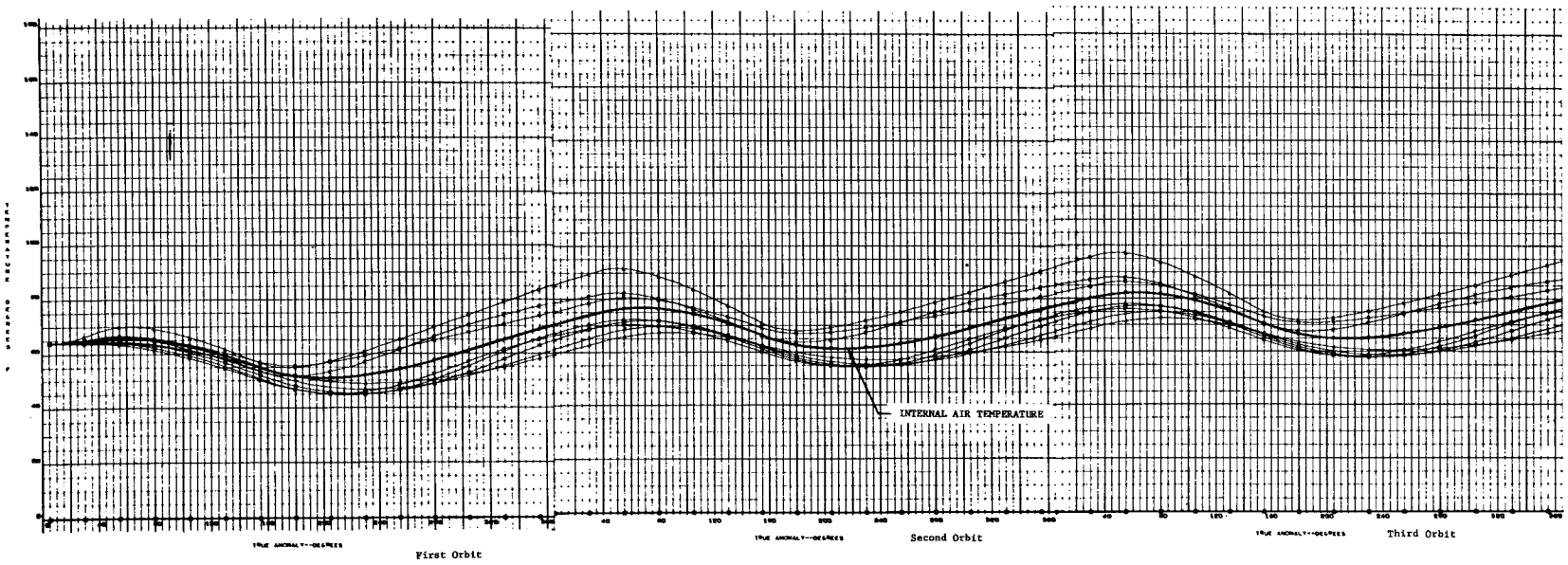

Figure 12. Internal Temperatures

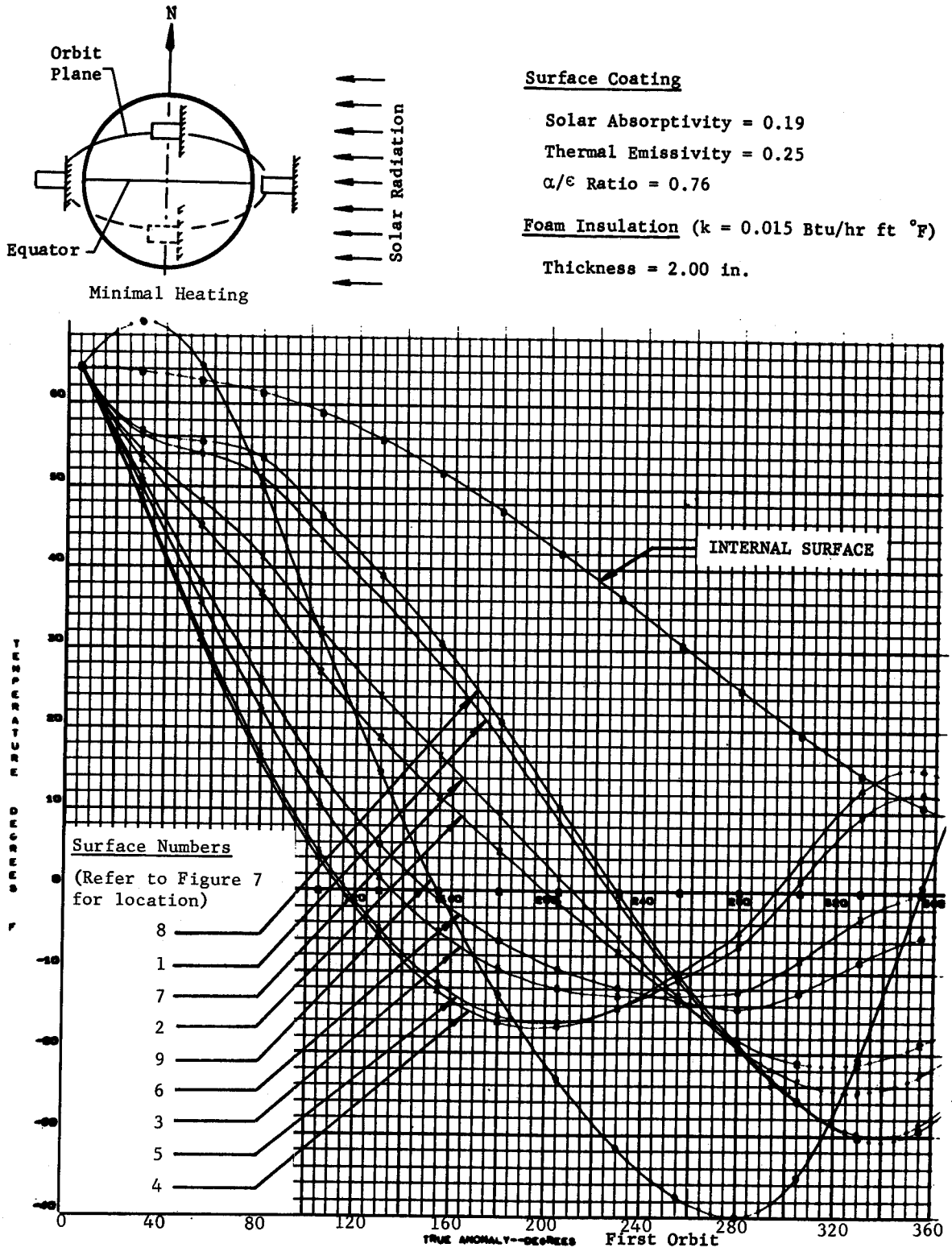

Figure 13. External Surface Temperatures

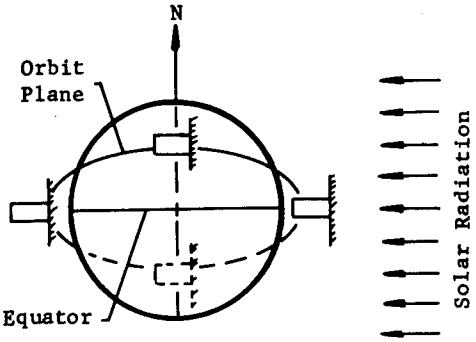

Surface Coating

Solar Absorptivity = 0.19

Thermal Emissivity = 0.25

α/ϵ Ratio = 0.75

Foam Insulation (k = 0.015 Btu/hr ft °F)

Thickness = 2.00 in.

Minimal Heating

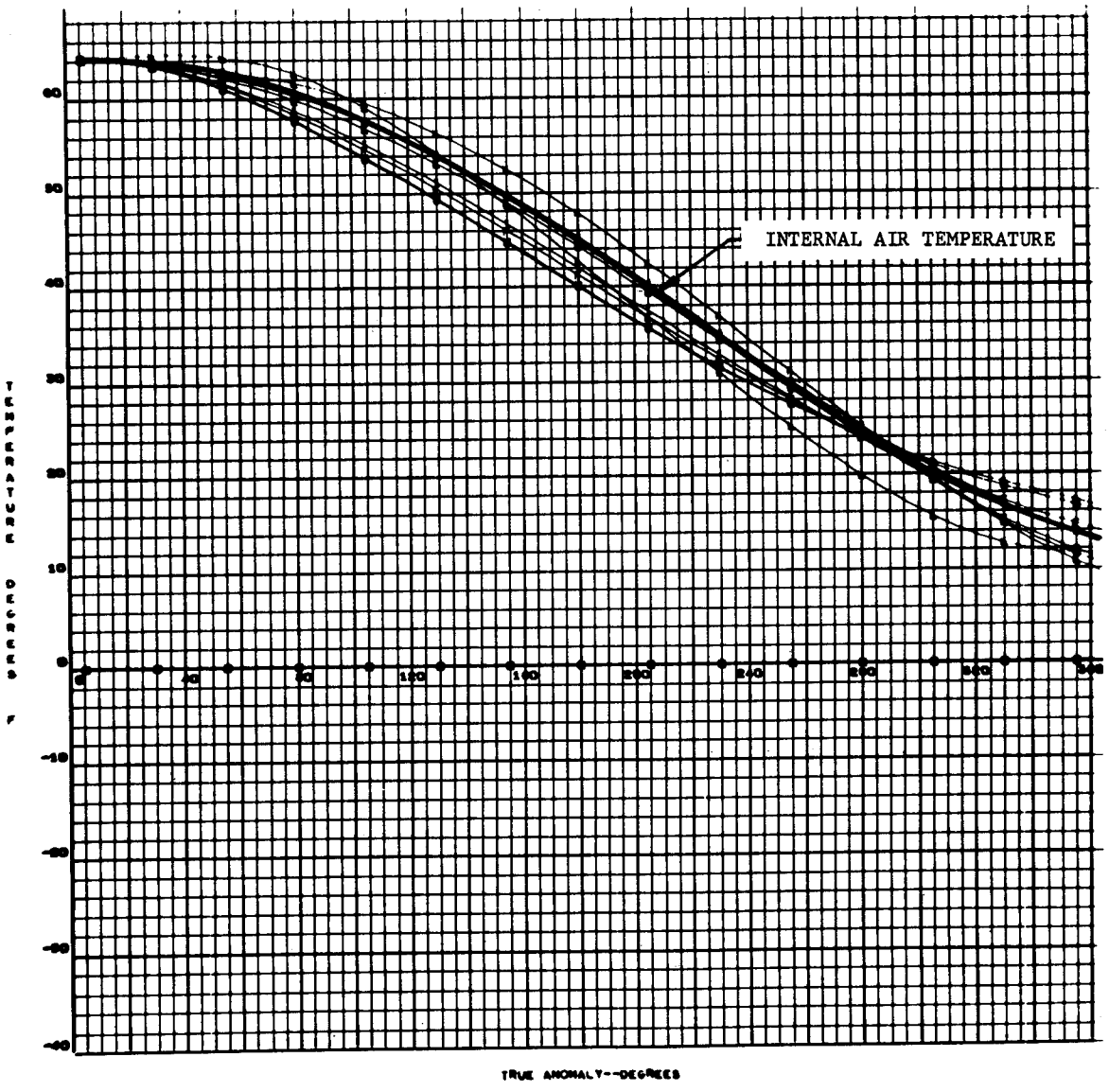

Figure 14. Internal Temperatures

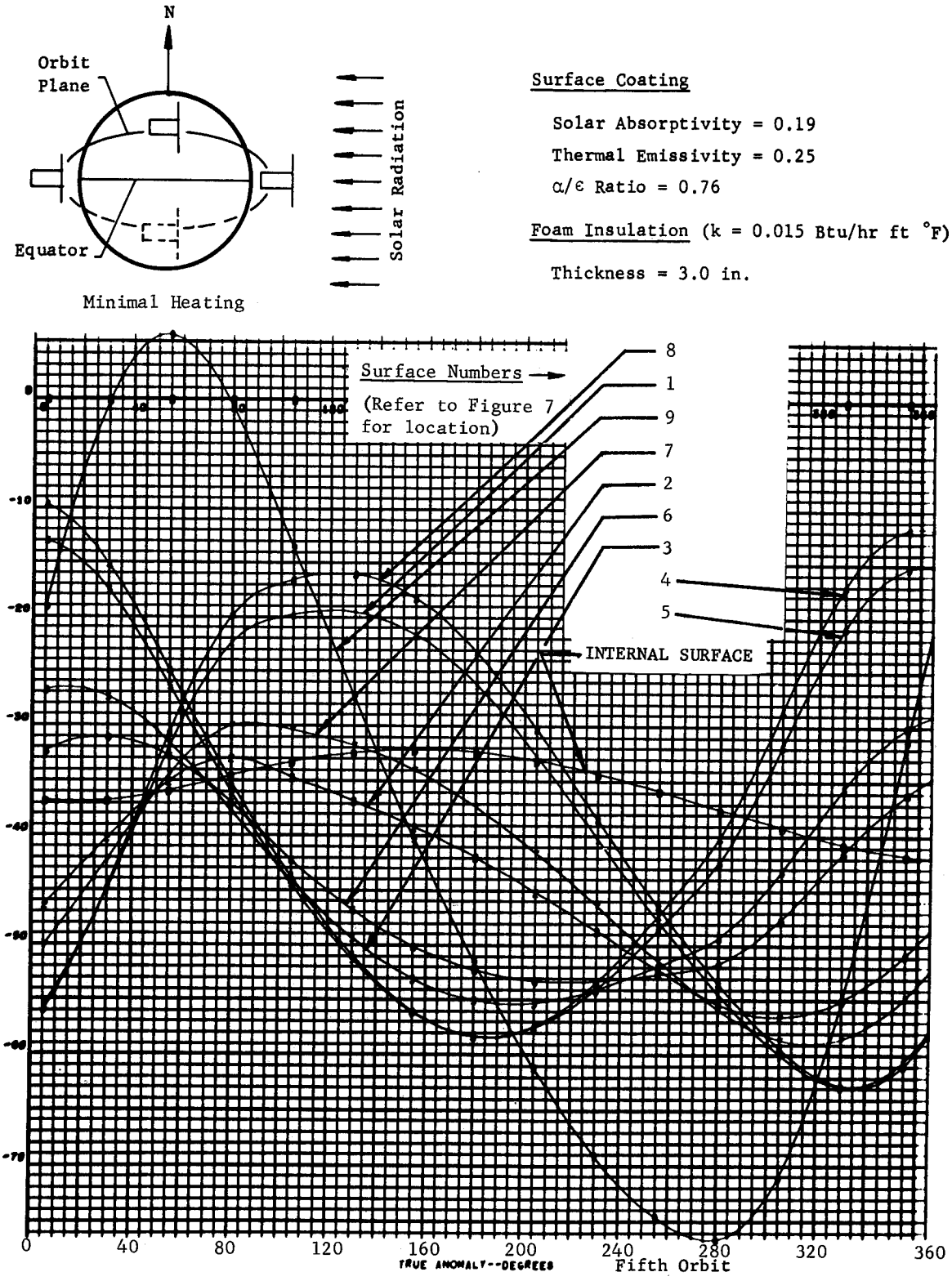

Figure 15. External Surface Temperatures

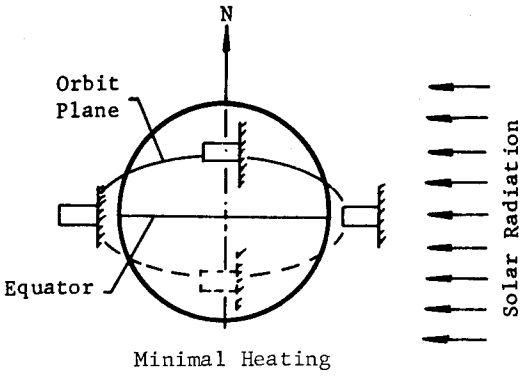

Minimal Heating

Surface Coating

Solar Absorptivity = 0.19

Thermal Emissivity = 0.25

α/ϵ Ratio = 0.76

Foam Insulation (k = 0.015 Btu/hr ft °F)

Thickness = 3.0 in.

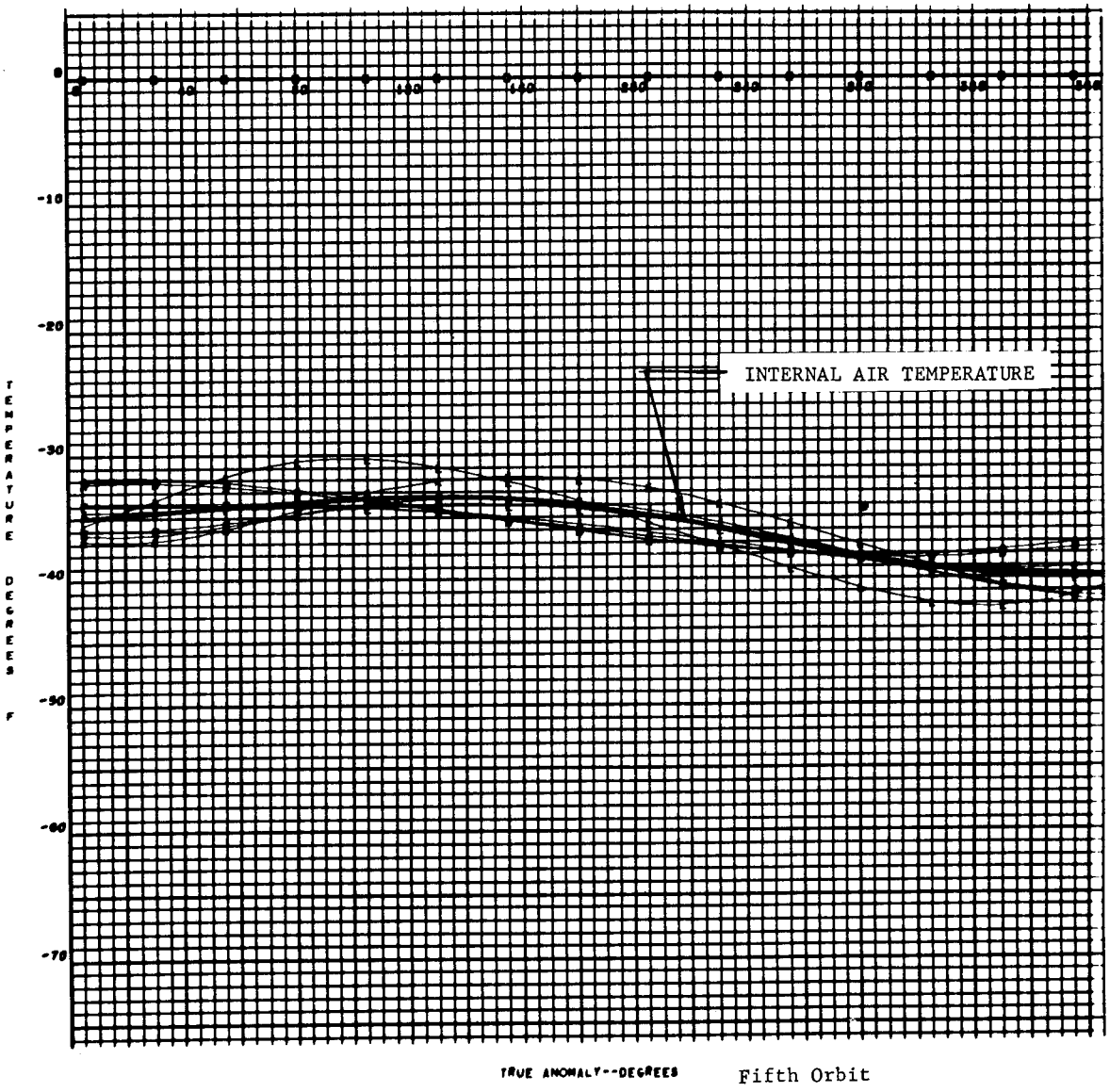

Fifth Orbit

Figure 16. Internal Temperatures

Coatings Nos. 5 and 6 provide the best passive temperature control for the airlock. The solar absorptivity and thermal emissivity values used for these two surfaces do not represent actual measured properties of physical surfaces. However, it is estimated that the polished aluminum or copper foil with a very thin layer of Teflon FEP outer surface would have spectral properties similar to Coatings Nos. 5 and 6.

Spectral reflectance measurement of surface material specimens should be conducted to determine solar absorptivity and thermal emissivity properties of commercially available materials compatible with the expandable airlock design.

V. DESIGN OF STRUCTURAL FABRIC*

An optimal design of a filamentary structure requires isotensoid fiber orientation; i.e., the fibers lay along geodesic paths and transmit loads in tension only. In the case of a structure that folds, the fibers must retain the designed orientation while the structure is expanded. Therefore, a matrix must be provided to maintain fiber orientation.

For the present airlock concept, a bellows-type configuration was chosen to provide foldability. This type of folding appeared best suited since the inherent foldability of the structural fabric would be restricted by the addition of outer protective layers as well as an inner liner. A bellows shape would be built into the load-carrying structure as shown in Figure 17. The appropriate fiber orientation for this design consists of a layer of longitudinal fibers to carry axial loads, with hoop fibers spaced along the cylinder to carry hoop loads. Since hoops can be filament wound with a resin, they do not require a knitted matrix to maintain the individual fiber spacing. However, the longitudinal fibers must be spaced uniformly to provide a substructure for the air-sealing liner.

The following discussion delineates filamentary structures applicable to an airlock as indicated by Reference 7.

A. Types of Structural Fabrics

1. Filament-Wound Structure

A corrugated airlock could be fabricated as a helically wound cylinder using an isotensoid design. This approach initially appeared attractive, since a helically wound cylinder constitutes one of the most efficient structures; i.e., the lightest weight for a given pressure load, when used as a pressure vessel. However, this approach was considered impractical for the present airlock requirements because of the following limitations.

In order to filament wind a corrugated cylinder, elaborate procedures would be required, including winding over a removable mandrel. In addition, the filaments would then have to be embedded in a matrix in order to maintain filament orientation. This would stiffen the structure and add difficulties to the folding process. For these reasons, alternative fabrication processes were considered.

2. Knitted Structure

There are basically two advantages of a knitted structure over a filament-wound structure: (1) a knitted structure is easier to fabricate, and (2) no matrix is required and therefore the structure has maximal flexibility. However, there is a weight penalty with a knitted structure, since the fibers lose about 30% of their strength when bent sharply. Also, fabrication tolerances are harder to control.

---

* This work was performed by Astro Research Corporation.

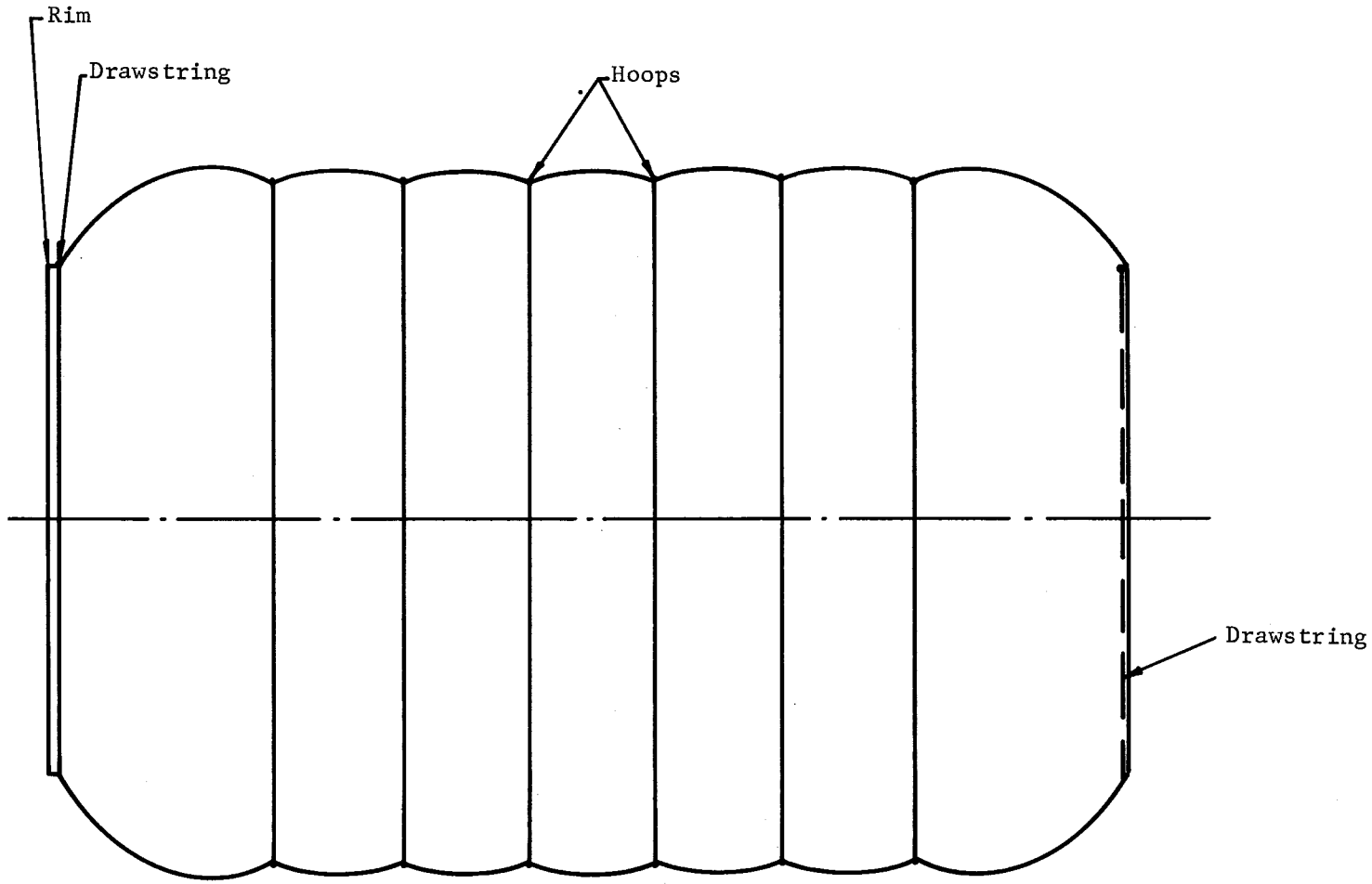

Figure 17. General Shape of Airlock Structure

3. Filament-Reinforced Knitted Structure

This concept, developed previously by Astro Research Corporation, involves a knitted structure that is used simply as a matrix to position filaments in a "filament-wound" structure. This construction is depicted in Figure 18. With this approach, a minimal weight knitting can be chosen, with all load carried by the added filaments. The advantages of this construction are (1) the load-carrying filaments are not subject to the decrease in strength from sharp bending that occurs in knitted structures, and (2) the knitted structure is made from light, easily worked filaments, with the heavy, load-carrying filaments simply laid in place. The weight of the knitted matrix is estimated to be 20% of the load carrying filaments.

4. Proposed Load-Carrying Structure

The filament-reinforced knitted construction offers significant advantages over both filament-wound and simple knitted construction. These advantages include fabricability, flexibility, and structural efficiency. This construction was therefore considered optimum for the airlock.

The load-carrying structure would consist of filament-reinforced knitted fabric to carry axial loads, with added hoop rings carrying hoop loads. A third major structural element in the system, as shown in Figure 17, would be drawstrings used to attach the load-carrying structure to the space station and to the entry port.

B. Structural Analysis

This analysis was taken from Astro Research Corporation Report No. ARC-R-169 (Reference 8).

1. Equilibrium Requirements for Longitudinal Fibers

The equilibrium conditions on a longitudinal fiber in the airlock structure can be obtained by taking a free-body section normal to the axis, as shown in Figure 19.

It can be seen that equilibrium demands that

$$nT \cos \alpha = p \pi r^2 \qquad (1)$$

where n = number of longitudinal fibers

T = tension in the longitudinal fibers

r = radius

α = slope angle of longitudinal fibers

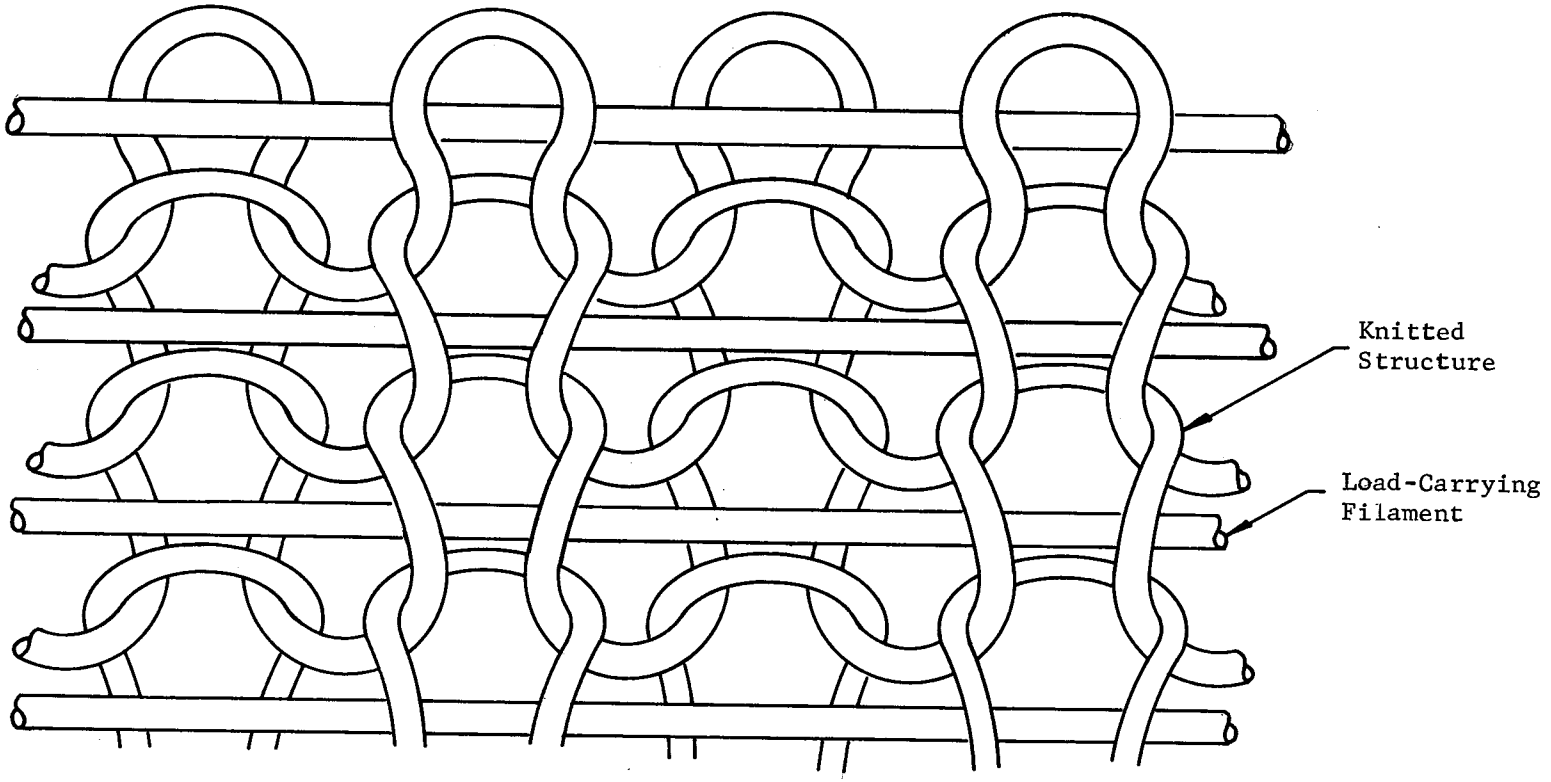

(b) Side View

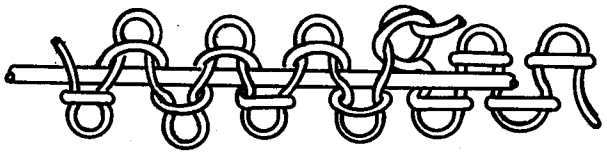

(a) Top View (Reduced)

Figure 18. Combined Knitting and Filament-Wound Structures

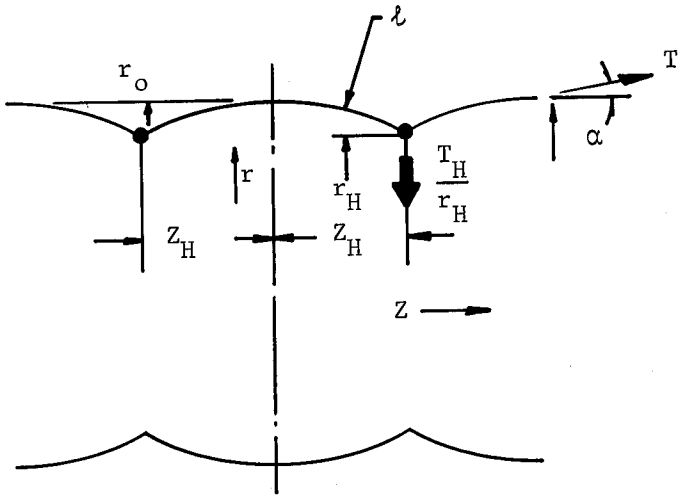

Figure 19. Equilibrium Conditions on Longitudinal Fiber

Also,

$$nT = p \pi r_o^2 \tag{2}$$

Then from equations (1) and (2),

$$\cos \alpha = \left(\frac{r}{r_o}\right)^2 \tag{3}$$

2. Solution for Equilibrium Shape of Meridian

Equation (3) establishes the requirement for the equilibrium shape of the meridian curve of the pressure vessel. In Reference 9, a more general form of this equation is integrated to obtain a closed-form solution in terms of the tabulated elliptic integral. As applied to equation (3), the results are as follows:

For the axial coordinate Z:

$$Z(r) = \frac{r_o}{\sqrt{2}} \{2E(\psi, k) - F(\psi, k)\} \tag{4}$$

where $F(\psi, k)$ = elliptic integral of the first kind

$E(\psi, k)$ = elliptic integral of the second kind

$k = \sin 45°$

$$\psi = \sin^{-1} \sqrt{1 - \left(\frac{r}{r_o}\right)^2}$$

For the arc length ℓ:

$$\ell(r) = \frac{r_o}{\sqrt{2}} F(\Psi, k) \tag{5}$$

Note that these quantities are measured from the point of maximal radius in either direction toward the hoop. Thus,

$$Z\left|r_o\right| = \ell\left|r_o\right| = 0$$

The tensile load in the hoops is related to the hoop spacing, since the spacing determines the angle of the corner pinched into the longitudinal fibers by the hoop. Figure 19 shows that the distance between adjacent hoops is $2Z_H$. If the axial coordinate of the drawstring is Z_D, then the length of the tube is

$$Z = 2Z_D + 2 m Z_H \tag{6}$$

where m is the number of hoops. Note that if Z and m are given, then Z_D and Z_H must be calculated to satisfy equation (6).

For the present problem, the assumption will be that the inside diameters of the hoop and drawstring are given, and that the outside diameter of the tube must be chosen in order to satisfy the requirements of equation (6). Thus, r_o must be determined so that equation (6) is satisfied, where Z_D and Z_H are determined from equation (4), with r_D and r_H predetermined. Because Z is an implicit function of r_o, this can best be accomplished numerically, by assuming various values of r_o and working through to find Z.

Figure 20 is a plot of r_o versus Z for various values of m.

From this set of curves, a value for r_o can be chosen which will correspond to the desired tube length.

The length of the longitudinal fibers is determined by adding the lengths of the arcs, from equation (5), that comprise the meridional curve. This total length L is given by

$$L = 2\ell_D + 2 m \ell_H \tag{7}$$

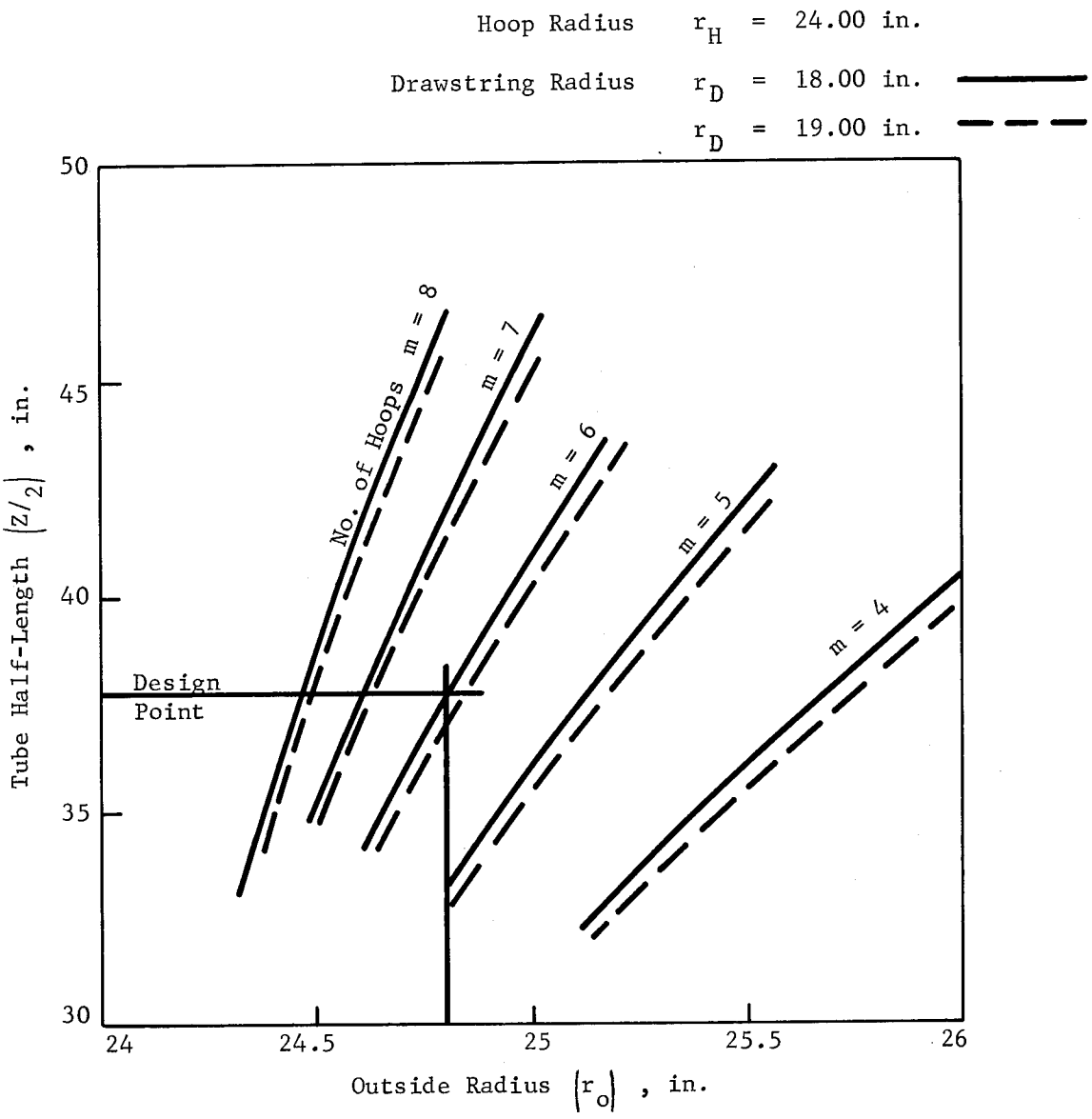

Figure 20. Effect of Outside Diameter on Tube Length

3. Conditions on Circumferential Hoops

Given the proper r_o, it is possible to compute the tension in the hoop and drawstring. The equilibrium requirements for a section of the hoop are shown in Figure 21:

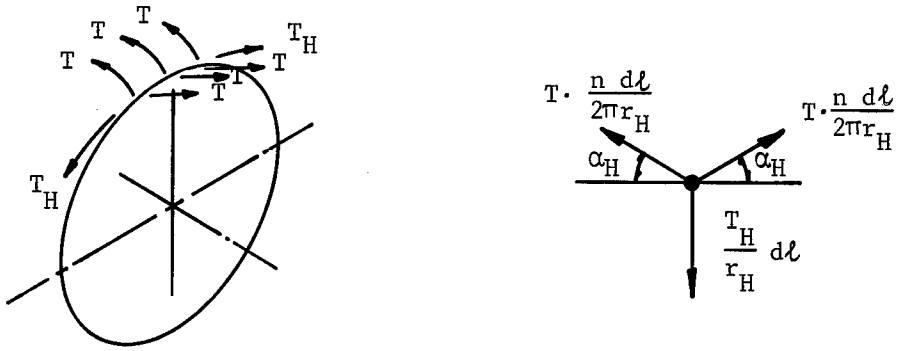

Figure 21. Equilibrium for a Hoop

The hoop tension forces T_H on a length $d\ell$ can be resolved into a radially inward-directed force $\frac{T_H}{r_H} d\ell$. This force must balance the radial component of the tension in associated meridional fibers; or

$$\frac{T_H}{r_H} d\ell = 2\, T \sin \alpha_H \cdot \frac{n\, d\ell}{2\, \pi\, r_H}$$

or

$$T_H = \frac{nT \sin \alpha_H}{\pi} \qquad (8)$$

where α_H is given by equation (3) at $r = r_H$:

$$\cos \alpha_H = \left(\frac{r_H}{r_o}\right)^2$$

4. Conditions at Ends of Tube

At the ends of the airlock, the fibers are turned into a radial plane by the rim on which the drawstring is mounted, as shown in Figure 22(a).

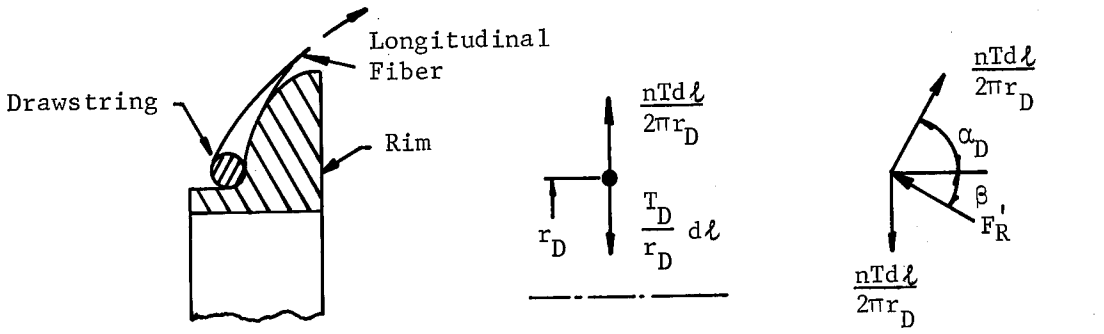

(a) Rim Detail (b) Drawstring Forces (c) Rim Forces

Figure 22. Rim and Drawstring Forces

The drawstring forces are therefore as shown in Figure 22(b). Equilibrium on a differential element of the drawstring gives

$$\frac{T_D}{r_D} d\ell = \frac{n\ T\ d\ell}{2\ \pi\ r_D}$$

or

$$T_D = \frac{n\ T}{2\ \pi} \tag{9}$$

The rim load, F_R', shown in Figure 22 (c), is

$$F_R'\ d\ell = 2\ \frac{n\ T\ d\ell}{2\ \pi\ r_D}\ \cos\left(\alpha_D + \beta\right)$$

or

$$F_R' = \frac{n\ T}{\pi\ r_D}\ \cos\left(\alpha_D + \beta\right) \tag{10}$$

where

$$\beta = \frac{1}{2}\left(\frac{\pi}{2} - \alpha_D\right)$$

Note that the rim load has a radial component which imposes a compressive load on the rim.

C. Design Data for Airlock Structure

The following design data were used for this design study.

1. General requirements:

Design internal pressure	10 psi
Safety factor	5
Hoop diameter	48 in.
Drawstring diameter	36 in.
Length between drawstrings	≈76 in.
Number of hoops	6

2. Longitudinal Fibers

Material	Heat-stretched Dacron
Breaking load per fiber	100 lb
Tension at design pressure	20 lb
Elongation at design pressure	2.0%
Specific strength	2.4×10^6 in.

D. General Dimensions for Airlock Structure

The calculations presented herein are based on the results of the analysis presented in Section V.B, and equation numbers refer to the equations derived therein. The general arrangement of the structure is shown in Figure 23.

1. Outside Diameter

Figure 20 shows that for six 48-in. hoops and 36-in. drawstrings, an outside radius of 24.80 in. gives a value of half-length of 37.85 in., which satisfies the requirement for a length of approximately 76 in. This point will be taken to represent the structure.

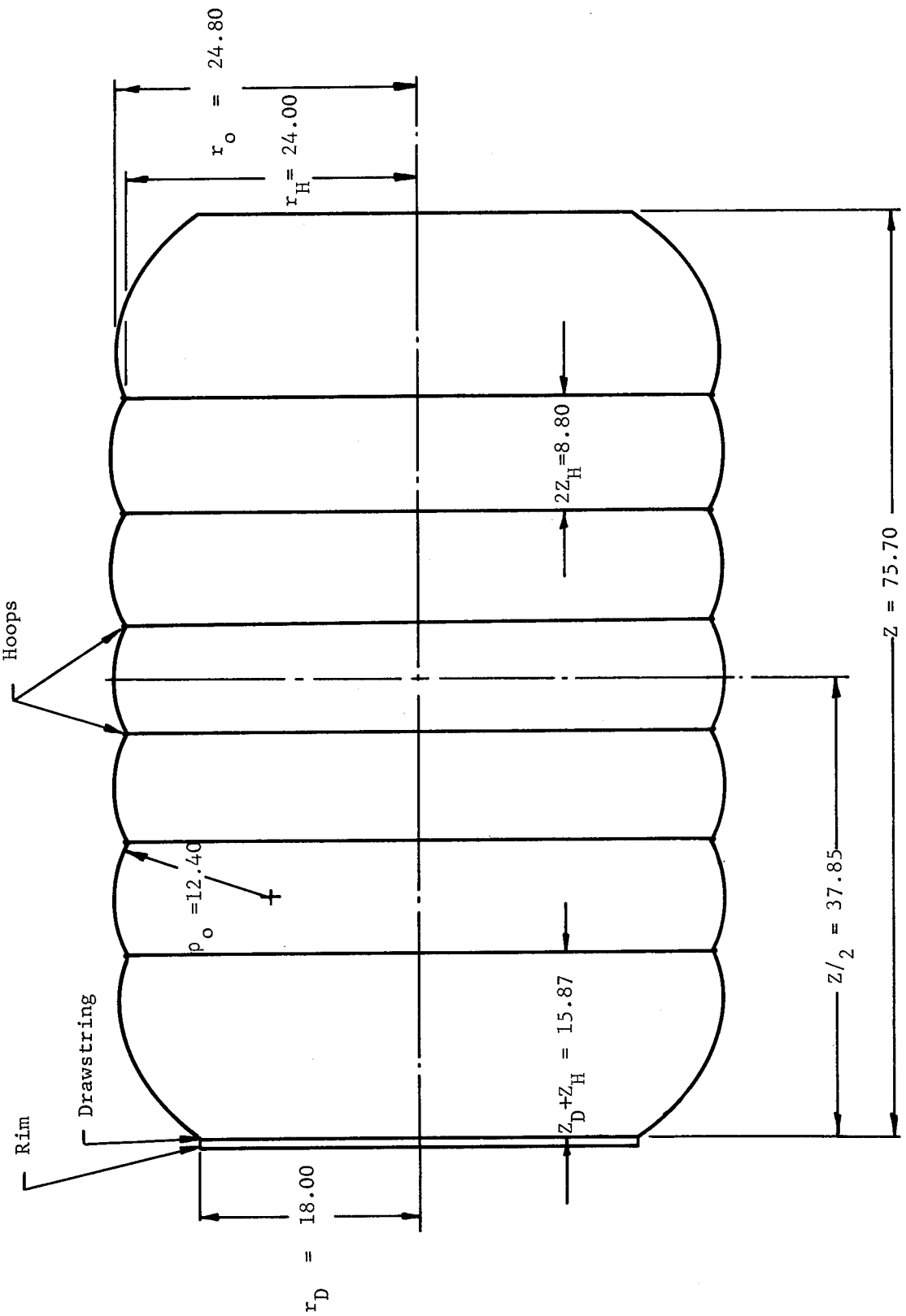

Figure 23. General Arrangement of Airlock Structure

Thus:

$$r_o = 24.80 \text{ in.}$$

$$r_H = 24.00 \text{ in.}$$

$$r_D = 18.00 \text{ in.}$$

$$Z = 75.7 \text{ in.}$$

2. Meridian Angles

Given r_o, the slope of the meridian may be calculated from equation (3):

$$\cos \alpha = \left(\frac{r}{r_o}\right)^2$$

At the hoop,

$$\cos \alpha_H = \left(\frac{24.00}{24.80}\right)^2 = 0.93652$$

$$\alpha_H = 20.52°$$

At the drawstring,

$$\cos \alpha_D = \left(\frac{18.00}{24.80}\right)^2 = 0.52678$$

$$\alpha_D = 58.21°$$

3. Hoop Spacing

The axial distance Z_H and the arc length ℓ_H from the crest to the hoop can be computed from equations (4) and (5). For the variables ψ and k corresponding to the hoop position on the meridian,

$$\psi_H = \sin^{-1} \sqrt{1 - \left(\frac{r_H}{r_o}\right)^2} =$$

$$= \sin^{-1} \sqrt{1 - \frac{24.00}{24.80}^2} = 14.61°$$

Also,

$$k = \sin 45°$$

From Reference 10, the values of F (ψ, k) and E (ψ, k) for these values are found to be

$$F_H = 0.25641$$

$$E_H = 0.25359$$

This gives for Z_H, from equation (4),

$$Z_H = \frac{r_o}{\sqrt{2}} \left\{2 E_H - F_H\right\}$$

$$= \frac{24.80}{\sqrt{2}} \{2 (0.25359) - 0.25641\}$$

$$= 4.398 \text{ in.}$$

For ℓ_H, from equation (5),

$$\ell_H = \frac{r_o}{\sqrt{2}} F_H$$

$$= \frac{24.80}{\sqrt{2}} (0.25641)$$

$$= 4.496 \text{ in.}$$

The spacing between hoops is $2Z_H$ for the axial distance and $2\ell_H$ for the arc length.

4. Drawstring Spacing

The axial distance Z_D and the arc length ℓ_D between the crest and the drawstring position on the meridian can be computed for the hoop. The values corresponding to the drawstring position are

$$\psi_D = 43.47°$$

$$k = \sin 45°$$

$$F_D = 0.79561$$

$$E_D = 0.72473$$

$$Z_D = 11.47 \text{ in.}$$

$$\ell_o = 13.95 \text{ in.}$$

5. Overall Length

The axial spacing between the drawstrings at the ends of the tube is given by equation (6):

$$Z = 2 Z_D + 2 m Z_H$$

$$= 2 (11.47) + 2 (6) (4.398)$$

$$= 75.7 \text{ in.}$$

The total length of longitudinal fiber between drawstrings is given by equation (7):

$$L = 2 \ell_o + 2 m \ell_H$$

$$= 2 (13.95) + 2 (6) (4.496)$$

$$= 81.85 \text{ in.}$$

E. Detail Design for Airlock Structure

Having determined the geometry of the structure, the structural loads and the sizes of the members needed to carry these loads may be determined.

1. Longitudinal Fibers

From equation (2), the total axial force at the design pressure can be written as

$$nT = p \pi r_o^2$$

$$= 10 \cdot \pi \cdot (24.80)^2 = 19{,}320 \text{ lb}$$

For a working tension of 20 lb per fiber, then, the number of longitudinal fibers required is

$$n = \frac{19{,}320}{T} = \frac{19{,}320}{20} = 966 \text{ fibers}$$

The fiber spacing at any radius is $\frac{n}{2\pi r}$ fibers/in.

At the outside, $\frac{n}{2\pi r} = 6.20$ fibers/in.

At the hoop, 6.40 fibers/in.

At the drawstring, 8.54 fibers/in.

Assuming a 2.0% working elongation, the free length of the longitudinal fibers is

$$L(1 - \epsilon) = 81.85 (1 - 0.02) = 80.21 \text{ in.}$$

The weight of the longitudinal fibers can be computed from the weight per unit length of the fiber. Assuming the Dacron fiber to have a specific strength λ of 2.4×10^6 in., the weight per unit length is

$$\frac{\omega}{\ell} = \frac{T}{\lambda} = \frac{100 \text{ lb}}{2.4 \times 10^6 \text{ in.}} = 0.38 \times 10^{-4} \text{ lb/in.}$$

The total length of fiber in the structure is

$$nL = 966\ (80.21) = 77{,}500 \text{ in.}$$

The weight of the longitudinals is therefore

$$W_L = \frac{\omega}{\ell} \cdot nL = \left|0.38 \times 10^{-4}\right| (77{,}500)$$

$$= 2.9 \text{ lb}$$

2. Hoops

The load in the hoops is given by equation (8):

$$T_H = \frac{n\ T \sin \alpha_H}{\pi}$$

$$= \frac{(19{,}320)(\sin 20.52°)}{\pi}$$

$$= 2{,}155 \text{ lb}$$

For a nominal design load of high-strength steel fibers of 1.5 lb, the number of turns required for each hoop is

$$n_H = \frac{T_H}{1.5} = \frac{2{,}155}{1.5} = 1{,}437 \text{ turns}$$

The cross-sectional area for the hoop can be estimated by assuming the area to be 85% steel. For a working stress of 120,000 psi, the area is

$$A_H = \frac{1}{0.85} \frac{T_H}{S} = \frac{2{,}155}{0.85\ (120{,}000)} = 0.0211 \text{ in.}^2$$

The shape required for the cross section is shown in Figure 24.

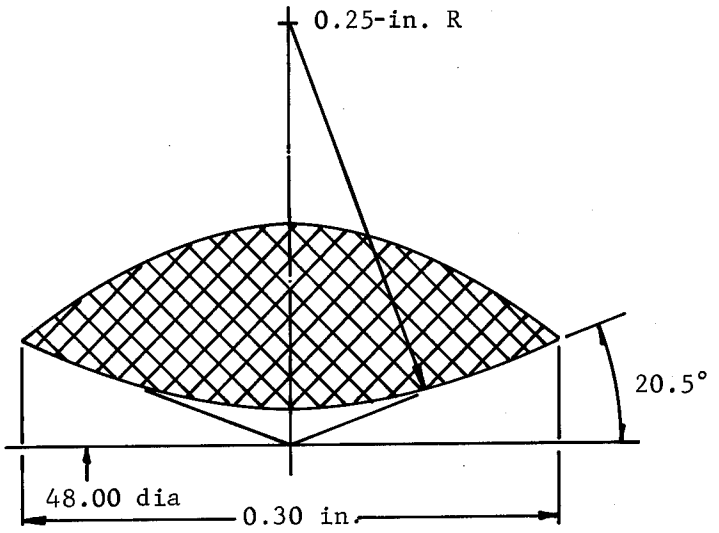

Figure 24. Cross-Sectional Detail for Hoop
(Scale: 10 times full size)

The weight of the structural fiber in the hoop can be computed from the volume of steel in the hoop

$$W_H = \gamma_S \cdot 2\pi r_H \cdot 0.85A_H$$

$$= 0.286 \cdot 2\pi (24.00) \cdot 0.85 (0.0211)$$

$$= 0.77 \text{ lb}$$

The additional weight of matrix in the hoop (compared to the weight of steel) is

$$\frac{\Delta W_H}{W_H} = \frac{\gamma_M}{\gamma_S} \cdot \frac{0.15}{0.85} = \frac{0.045}{0.286} \cdot \frac{0.15}{0.85} = 0.028, \text{ or approximately } 3\%$$

The total weight of each hoop is then

$$W_H + \Delta W_H = 1.03\, W_H = 1.03\ (0.773)$$

$$= 0.80 \text{ lb}$$

3. Drawstrings

The load in the drawstrings is given by equation (9):

$$T_D = \frac{n\,T}{2\,\pi}$$

$$= \frac{19,320}{2\,\pi} = 3,075 \text{ lb}$$

For a design load of 1.5 lb per fiber, the number of turns required is

$$n_D = \frac{T_D}{1.5} = 2,050 \text{ turns}$$

The cross-sectional area, assuming 85% steel, is

$$A_D = \frac{1}{0.85}\,\frac{T_D}{S} = \frac{1}{0.85}\,\frac{3,075}{120,000} = 0.0301 \text{ in.}^2$$

The shape required for the cross section is shown in Figure 25.

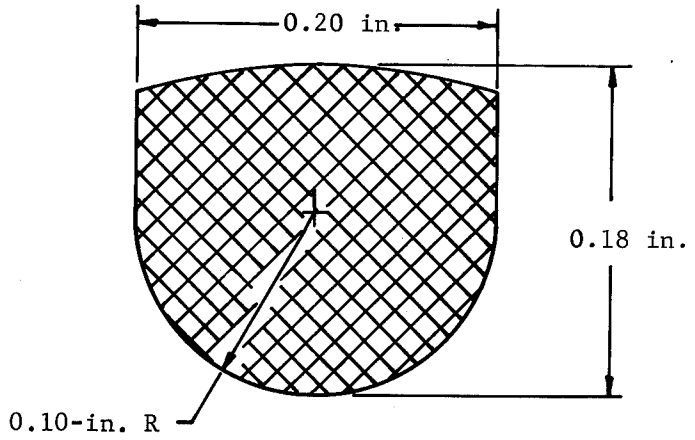

Figure 25. Cross-Sectional Detail for Drawstring (Scale: 10 times full size)

The weight of steel fiber in the drawstring is

$$W_D = \gamma_S \cdot 2\pi r_D \cdot 0.85 A_D$$

$$= 0.286 \cdot 2\pi (18.00) \cdot 0.85 (0.0301)$$

$$= 0.83 \text{ lb}$$

Assuming an additional weight of the matrix of 3%, the total weight of the drawstring is

$$W_D + \Delta W_D = 1.03 W_D = 1.03 (0.83)$$

$$= 0.85 \text{ lb}$$

Test data indicate the desirability of increasing the bend radius of the Dacron yarn around end-rings and hoops. This can be accommodated without increase in weight by substituting, for the steel wire rings specified previously, filament-wound glass rings of equal weight but of proportionately larger section.

Assuming a density ratio of glass/steel laminate of 0.08/0.25, the linear scale factor increase of the hoop and drawstring dimensions will be 1.77. The required equivalent uniaxial tensile strength in the hoop then becomes, for a safety factor of 5,

$$\frac{120{,}000 \times 0.85}{(1.77)^2} \times 5 = 163{,}000 \text{ psi}$$

High-quality filament glass rings will exceed this required value considerably. A typical value obtained for S-glass rings is 300,000 psi.

VI. METEOROID PROTECTION FOR THE EXPANDABLE AIRLOCK

A. Introduction

The purpose of this analysis was to determine the thickness required to provide protection from the expected meteoroid flux during the orbital mission. The procedure used for determining the composite thickness was developed from the studies originated under NASA sponsorship (Reference 1).

The analytical method assumed that each composite layer performed a function in preventing meteoroid penetration of the inner wall. The laminate layer of the composite would either fragment or stop the particles. The foam layer of the section would absorb the particles.

This analysis was developed to present an engineering approach to the protection afforded by a composite construction consisting of reinforced plastic and flexible foam core. However, due to the lack of data on this effect of hypervelocity impact upon orthotropic materials, the strength properties were assumed.

B. Analysis

1. Assumptions

The following assumptions were necessary to provide a starting point for the analysis.

a. The critical meteoroid mass was determined from data reviewed by the Air Force (Reference 11).

b. The material properties were estimated for typical elastic recovery materials.

c. Further assumptions have been noted in the analysis as required.

2. Nomenclature

A_p	Airlock projected area, ft^2
A_s	Airlock surface area, ft^2
K , F	Constants from Reference 11
L	Characteristic meteoroid length, in.
N	Meteoroid flux density, flux/ft^2 day
m_c	Critical meteoroid mass, gm

$P_{(x = 0)}$ Probability of no penetrations

S_p Meteoroid (i.e., projectile) shear strength, psi

S_t Facing or foam (i.e., target) shear strength, psi

T Mission time, days

t_f Outer facing or bumper skin thickness

t'_p Penetration depth in a thin plate

V Velocity of meteoroid, ft/second

V^*_f Velocity of faster fragment of shattered meteoroid, ft/second

V^*_s Velocity of slower fragments of shattered meteoroid, ft/second

$\bar{V}_c$, $\bar{V}_f$ Volume of slower and faster meteoroid fragments respectively, $in.^3$

Z $\frac{S_t \rho_t}{S_p \rho_p}$ bumper parameter

ρ Density of material, lbs/ft^3

ρ_p Density of particle, $lbs/in.^3$

3. Critical Meteoroid Properties

The following properties were assumed for determining the critical meteoroid:

a. Probability of no penetrations; $P_{(x = 0)} = 0.995$

b. The vehicle orbit of 200-natical miles

c. Airlock areas include:

A_p = projected area = DL = 4 x 7 = 28 ft^2

A_s = exposed area = π DL = 3.14 x 4 x 7 = 88 ft^2

d. Time in orbit was assumed to be one year

From Reference 11, the general interference factor was given as:

$$S_F = S_E S_I$$

where S_F = total interference factor

S_E = earth shield factor

From Figure 6 of Reference 11, the values for S_E and S_I for the assumed orbit were given as:

$$S_E = 0.65$$

$$S_I = 1.0 \quad \text{(No components that shield the airlock)}$$

$$\therefore S_F = 0.65$$

The form factors for the airlock shape were also taken from Reference 11 and apply for a particle mass less than 10^{-2} gm. The factors were:

$$K = 1.0$$

$$F = 0.44$$

Using these parameters, the meteoroid flux density was obtained from the following equation.

$$N = \frac{1 - P_{(x = 0)}}{S_F \, (K A_s + F A_p) \, T}$$

$$= \frac{1 - 0.995}{0.65 \, (1.0 \times 88 + 0.44 \times 28) \, 365}$$

$$\therefore N = 0.21 \times 10^{-6} = 2.1 \times 10^{-7} \text{ flux/ft}^2 \text{ day}$$

$$\text{Log}(N) = \text{Log}\ (2.1 \times 10^{-7}) = 0.322 - 7 = -6.678$$

$$\text{Log}\ N = -1.34\ \text{Log}\ (m_c) - 10.423 \quad \text{(Equation 6; Reference 11)}$$

$$-6.678 = -1.34\ \text{Log}\ m_c - 10.423$$

$$\text{Log}\ m_c = \frac{-6.678 + 10.423}{-1.34} = -2.8$$

Therefore the critical meteoroid mass is:

$$m_c = 1.585 \times 10^{-3}\ \text{gm}$$

With this information and that given in the references, the design meteoroid properties are defined as

*a. Particle density.

$$\rho_p = 2\ \text{gm/cm}^3 = 0.0725\ \text{lb/in.}^3$$

b. Particle velocity.

$$V = 30.5\ \text{km/sec} = 100{,}000\ \text{ft/sec}$$

} Reference 12

c. Particle volume.

$$\overline{V}_c = \frac{1.585 \times 10^{-3}}{454 \times 0.0725} = \frac{1.585 \times 10^{-3}}{32.9} = 0.0481 \times 10^{-3}$$

$$= 48.1 \times 10^{-6}\ \text{in.}^3$$

Assume the shape of a typical meteoroid is a sphere, as indicated in Reference 13. Then

$$\frac{4}{3}\pi R^3 = 48.1 \times 10^{-6}$$

$$R^3 = \frac{48.1 \times 10^{-6}}{4.18} = 11.5 \times 10^{-6}$$

* Note that this is a departure from the Reference 11 recommendation. By engineering judgement only, the Reference 12 value was considered best for this analysis.

d. $L = R = 2.26 \times 10^{-2} \approx 0.023$ in. (assume)

e. From the literature, most investigators assume a typical meteoroid is a glasslike composition. Then a reasonable assumption would be that the fracture strength of glass is representative of the meteoroid shear strength as required for this analysis. Thus assume the particle shear strength is 10,000 psi.

4. Composite Thickness Determination

For this preliminary analysis, only the penetration failure mode is used.

a. To compute t_f for first or outer facing, assume typical facing properties as

$$S_t = 7{,}700 \text{ psi}$$

$$\rho_t = 0.058 \text{ lb/in.}^3$$

The bumper parameter, Z , as defined in Reference 1 is then determined.

$$Z = \frac{S_t \rho_t}{S_p \rho_p} = \frac{7{,}700 \times 0.058}{10{,}000 \times 0{,}0725} = 0.615$$

From Figure 91 of Reference 1,

$$\frac{t_f}{t'_p} = 0.06$$

Then using equation (7) of Appendix D in Reference 1 as the penetration equation the outer facing of the composite can be found

$$t_f = 0.6\ (1.5)(0.97)\ V^{0.18}\ \rho_p^{0.26}\ \rho_t^{-0.46}\ S_t^{-0.04}\ V_c^{1/3}$$

$$= 0.0874\ (100{,}000)^{0.18}\ (0.0725)^{0.26}\ (0.058)^{-0.46}\ (7{,}700)^{-0.04}\ \left|48.1 \times 10^{-6}\right|^{1/3}$$

$t_f = \underline{0.033 \text{ in.}}$ (thickness of outer facing)

b. The determination of the foam thickness, based upon the velocities of particle fragments is determined next.

To find V_f^* V_s^* (velocities of fast and slow fragments):

From Figure 92 of Reference 1, for

$$\frac{\text{Wt. shield/unit area}}{\text{Wt. of projectile/unit area}} = \frac{0.058\ (0.033)}{0.0725\ (0.023)} = 1.15$$

$$V_f^* = 1.15 \times 100{,}000 = 115{,}000 \text{ ft/sec}$$

$$V_s^* = 0.1 \times 100{,}000 = 10{,}000 \text{ ft/sec}$$

The equivalent density of fragments is found from the average density of the facing and impacting particle.

$$\rho_E = \frac{\rho_t + \rho_p}{2} = \frac{0.058 + 0.0725}{2} = 0.065 \text{ lb/in.}^3$$

From Figure 93 of Reference 1 and with $Z = 0.615$

$$\frac{t_f}{L} \frac{\bar{V}_f}{\bar{V}_{orig.}} = 8 \times 10^{-3}$$

$$\frac{0.033}{0.023} \frac{\bar{V}_f}{48.1 \times 10^{-6}} = 8 \times 10^{-3}$$

$$\bar{V}_f = \frac{48.1 \times 10^{-6} \times 8 \times 10^{-3}}{1.43} = 268 \times 10^{-9} \text{ in.}^3$$

for a velocity of 20,000 ft/sec

To find the volume of the fast particles ($V = 100{,}000$ ft/sec) following form is used.

$$V_{f_{(V = 100{,}000 \text{ ft/sec})}} = V_{f_{(20{,}000 \text{ ft/sec}}} \left(\frac{V^{*0.18}}{(20{,}000)^{0.449}} \right)$$

$$= 268 \times 10^{-9} \times 0.092$$

$$= \underline{24.6 \times 10^{-9} \text{ in.}^3}$$

The Core thickness is determined from the following penetration formula taken from Reference 1:

$$t'_p = 1.5\ (0.97)\ V^{0.18}\ \rho_E^{0.26}\ \rho_{tc}^{-0.46}\ S_{tc}^{-0.04}\ \bar{V}_f^{1/3}$$

Assume

$$\rho_E = 0.065\ \text{lb/in.}^3 \quad \text{(From page 65)}$$

and foam properties as

$$\rho_{tc} = 1.35\ \text{lb/ft}^3 = 0.000783\ \text{lb/in.}^3$$

$$S_{tc} = 40\ \text{psi} \quad \text{(core tensile strength)}$$

$$t'_p = 1.5\ (0.97)(115{,}000)^{0.18}\ (0.065)^{0.26}\ (0.000783)^{-0.46}\ (40)^{0.04}\ \left(24.6 \times 10^{-9}\right)^{1/3}$$

$$t'_p = \underline{0.387\ \text{in.}}$$

c. To determine the inner facing thickness required to absorb the slower fragments; the calculations used in the part b. are repeated with different material properties.

$$\frac{t_f}{L}\ \frac{\bar{V}_s}{\bar{V}_f} = 6$$

$\bar{V}_s$ = volume of slower fragments

Assume $\frac{t_f}{L} = 1.43$

$$\bar{V}_s = \frac{24.6 \times 10^{-9} \times 6}{1.43} = 99 \times 10^{-9}\ \text{in.}^3$$

Then with the following slow fragment properties the thickness of the inner facing is determined.

$$\rho_p = 0.065 \text{ lb/in.}^3$$

$$\rho_t = 0.058 \text{ lb/in.}^3$$

$$S_t = 7{,}700 \text{ psi}$$

$$V_s^* = 10{,}000 \text{ ft/second}$$

$$t_p' = 1.5\,(0.172)\,V^{0.893}\,\rho_p^{0.979}\,S_t^{-0.457}\,\rho_t^{-0.35}\,V_s^{1/3}$$

$$= 1.5\,(0.172)(10{,}000)^{0.893}\,(0.065)^{0.979}\,(7{,}700)^{-0.457}\,(0.058)^{-0.35}\,99 \times 10^{-9\,1/3}$$

Therefore, the thickness of the inner facing required to stop the slow fragments is:

$$t_p' = \underline{\underline{0.014 \text{ in.}}}$$

5. Summary of Composite Thickness

By engineering judgment only, apply a factor of safety to core thickness only

$$F.S. = 5$$

Then $t_c = 0.387 \times 5 = 1.935 \text{ in.} \cong 2.0 \text{ in.}$

For a preliminary design, then, the wall concept would be

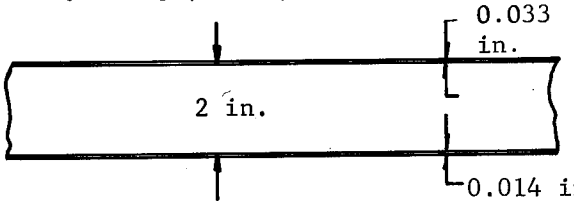

Wt./ft^2 of wall = $144 \times 0.058 \times 0.047 = 0.392$ lb/ft^2

$144 \times 2 \times \frac{1.35}{1{,}728} = \underline{0.225 \text{ lb/ft}^2}$

Total = 0.617 lb/ft^2

C. Discussion

The composite thickness determined for meteoroid protection was based on the method of analysis previously developed. This analysis has yet to be confirmed experimentally. Based on observation of the work performed by others, this analysis is probably conservative. Tests conducted in the velocity range of 12,000 to 30,000 ft/sec indicate that a thinner outer laminate would perform the same function as that calculated. Preliminary hypervelocity impact tests conducted by the Langley Research Center on composite wall samples, similar to those shown in Figure 2, with 10 milligram Mylar disks at velocities of approximately 7,000 and 18,000 ft/sec, indicate that a lower bumper weight may be sufficient. The analysis will be revised at a future date to incorporate factors which would reflect the micrometeoroid test results.

As a result of the tests, the bumper skin thickness would probably be reduced to save weight and also increase the flexibility of the composite. The reduction of the skin thickness would not excessively degrade the meteoroid protection afforded by the airlock system.

VII. RADIATION PROTECTION

A detailed investigation of the radiation protection was not made for this feasibility study, as the astronaut would not spend long periods of time in the airlock. If the space station were to pass through a radiation "storm," the astronaut would be within the protection afforded by the space station.

The effectiveness of elastic recovery materials against space radiation was discussed in Reference 1. This study experimentally determined the "effective atomic number," relative $\overline{Z}$, for the component materials of the elastic recovery composite. The test procedure utilized low-level sources in a low-pressure chamber. The $\overline{Z}$ was obtained from aluminum, which has a known atomic number and absorber characteristics. The aluminum sheet was used as the standard index. The elastic recovery materials were then compared with the index as shown in Table 7.

The lower the relative $\overline{Z}$ number, the more effective the material was in shielding against the corpuscular radiation. Table 7 also lists the material densities ρ.

The most important materials which apply to the expandable airlock design include the foam and Fortisan fabric laminate. It must be noted that the effect of long-term exposure of these flexible materials to space radiation is not known at this time.

TABLE 7

EFFECTIVE ATOMIC NUMBER AND DENSITY OF
ELASTIC RECOVERY MATERIALS

Material	Relative Z *	ρ g/cm^3**
Index reference standard aluminum	13.00	2.700
Aluminum on Mylar	12.23	1.315
Polyvinyl chloride (PVC) resin/181 glass fabric	11.34	1.680
PVC resin/Fortisan fabric	10.24	1.380
Polyurethane foam	9.13	0.237
PVC resin-carbon/181 glass fabric	8.80	1.395
Polyurethane foam-carbon	8.24	0.356
PVC resin-carbon/Fortisan fabric	8.02	1.280
DuPont type 46971 polyester adhesive	6.92	1.240

* Effective Atomic Number
** Density

VIII. FOLDING AND PACKAGING

The method for determining the best approach for folding the airlock was largely experimental. The complicating factor in the folding technique for the airlock was the requirement for multiple retraction and deployment cycles. Narmco felt that the best folding technique was a combination of random and forced folding points.

The use of the elastic recovery concept for the flexible wall of the airlock exhibits the best recovery characteristics when the foam has its greatest compression. To accomplish this requires many minor rather than a few major folds in the wall section. The use of many folds in the wall section also provides for faster deployment, since shallow creases "pop out" more easily than deep creases. These observations resulted from the series of test models which were made for this study.

A series of small-scale models were used to determine the folding characteristics of airlock. The primary disadvantage of the scale models was the lack of proper scaling laws for composite construction. The size of the models could and was reduced geometrically. However, wall stiffness could not be reduced accordingly. In view of this contradictory nature of scaling composite wall section, Narmco assumed only geometric scaling for the models and chose a 1/4-scale as representative of the compromise between full and small scale. This size produced a model which was 1 ft in diameter and 1-3/4 ft long. In order to achieve a similar stiffness of the wall, a scale of 1/2 was used resulting in a thickness of one inch.

The model study began with simple cylinders and progressed to more complex configurations. The more complex models included configurations with flexible or rigid bands and simulated convolutions.

The simple cylinder model is shown in the extended and folded positions in Figure 26. This cylinder was tested in a simple fixture which allowed the use of cables to fold the cylinder. The areas showing the surface of extended cylinder were the results of previous folding tests. The creases were the initiation points for the major folds as the cylinder was cycled. Some of the major folds or buckles were noted under the shroud in Figure 26 (b).

Two general approaches were then taken in the model study to determine if the major folds or buckles could be eliminated. The first approach was to segment the skin in a manner which would force the cylinder to fold into small, diamond-shaped buckles. The buckles were similar to those encountered in buckling of cylinders subjected to axial compression. This method would be necessary if a "stiff" skin would have been needed for protection.

This approach was applied to small (6-in.) diameter cylinders and apparently worked as predicted. However, the application to larger cylinders was not possible because the buckling characteristics for the composite wall could not be predicted accurately beforehand to determine the size of the diamond-shaped segments. The size of the buckle would depend on the shape and thickness

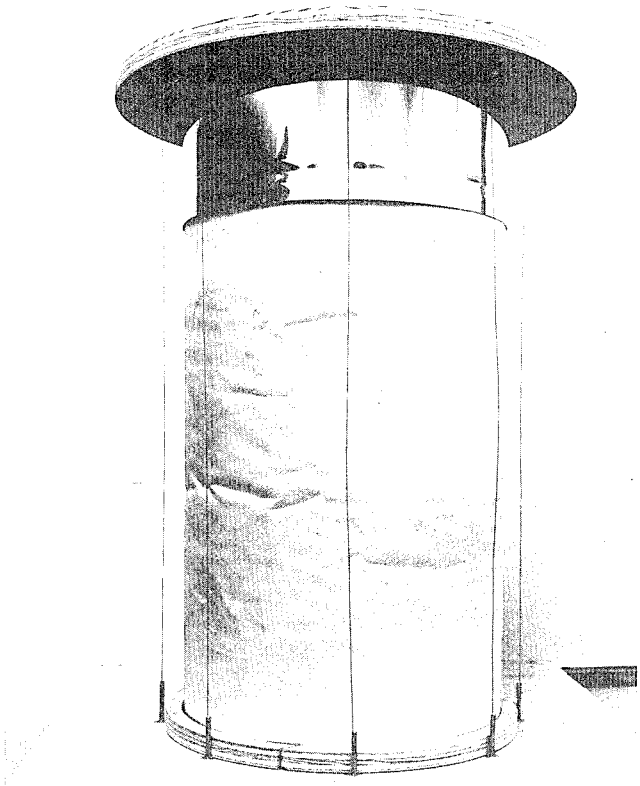

(a) Deployed

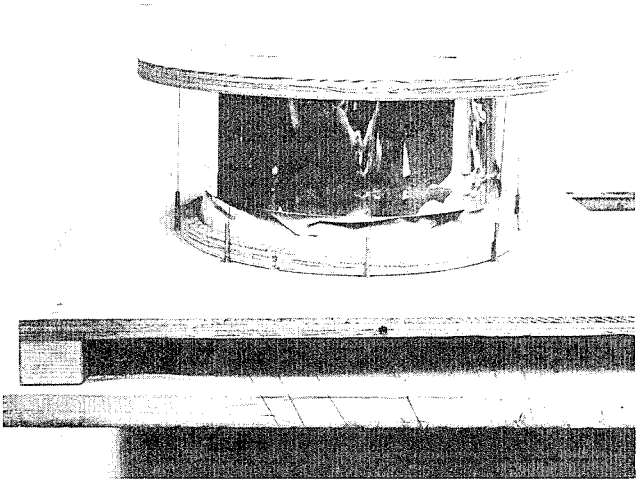

(b) Folded

Figure 26. Cylindrical Model in Fixture

of the cylinder as well as the composite material properties. An extensive study was not made of this technique, since extremely flexible skins were developed, thus eliminating the requirement.

The second approach to folding and packaging was to determine methods by which the creases could be minimized in the wall section. Hoop bands were placed along the length of the cylinder to see how the folding pattern would be modified. The cylinder shown in Figure 27 was made with bands cut from a 2-ply laminate. The folding pattern of the cylinder is shown by the sequence in Figure 28. The "flexible" bands had little effect on decreasing the large folds. The same cylinder was then folded without the bands, and the folding pattern was the same as before. Figure 29 shows the cylinder, without bands, partially and fully folded. The major folds or buckles were present in the wall.

The effect of rigid rings upon the folding characteristics of a one-quarter size model of the airlock was determined. For this experiment, rings wound with impregnated glass roving were made and assembled on the model. The extended and folded model is shown in Figure 30. The rings were effective in preventing the buckles from forming. The packaging was accomplished by compression of the material and also by small folds. This type of folding is the desired characteristic for the elastic recovery composite.

The use of rings with the flexible composite section is also compatible with the structural requirements for the airlock. For the full-scale airlock, hoop bands or rings are necessary to resist the circumferentials loads as was previously discussed.

A related area of investigation was that of determining the packaging loads and packaging ratio which could be expected with the expandable airlock system. This work was accomplished with a full-size diameter cylindrical section. The cylinder had a diameter of 4 ft and a length of 3 ft. The thickness of the wall was the same as required for the airlock. The cylinder was made without convolutions and bonded to circular end plates to ensure that the ends would remain circular, as shown in Figure 31.

Load was applied to the cylinder edge by means of weights suspended from the center of the top end plate. This means of suspension prevented the load from shifting in case the cylinder buckled on one side. Two loading cycles were run. During the first test, the cylinder did buckle on one side (see Figure 32) when the load reached 75 lb.

The bottom end plate was then modified with vertical pipe supports to prevent the large buckles from forming in the wall section. The top end plate was allowed to slide up and down the vertical supports. When the cylinder was loaded, it folded uniformly into a major circumferential buckle. This circumferential fold did not allow for as much material compression as would have been desired. The load deformation information was recorded until the maximal packaging was reached. This information is plotted in Figure 33. The deformation is the average of three readings around the circumference. The cylinder at its maximum load is shown in Figure 34.

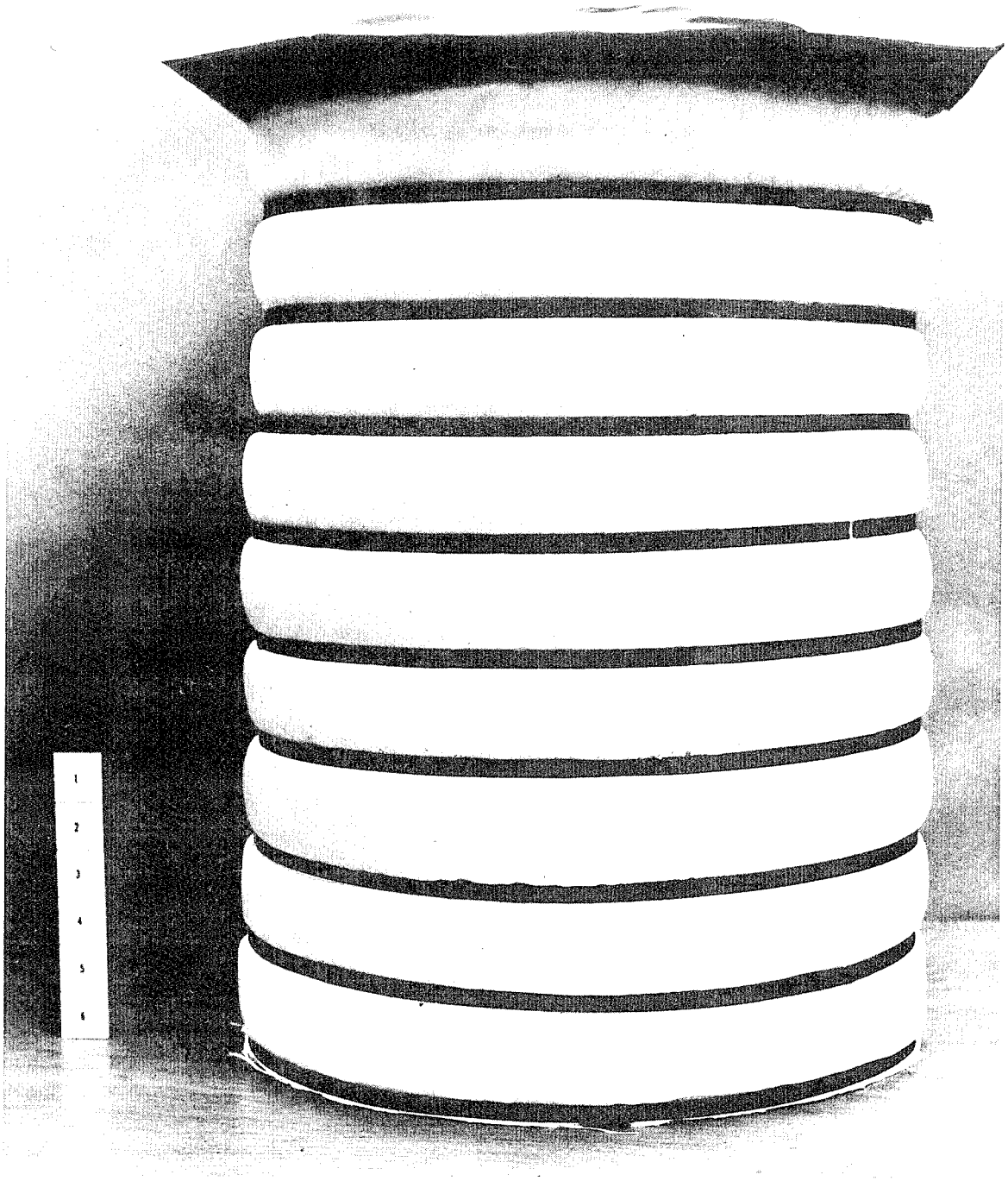

Figure 27. Cylindrical Cylinder
with Flexible Bands

(a)

(b)

(c)

Figure 28. Folding Sequence for the Cylinder with "Flexible" Bands

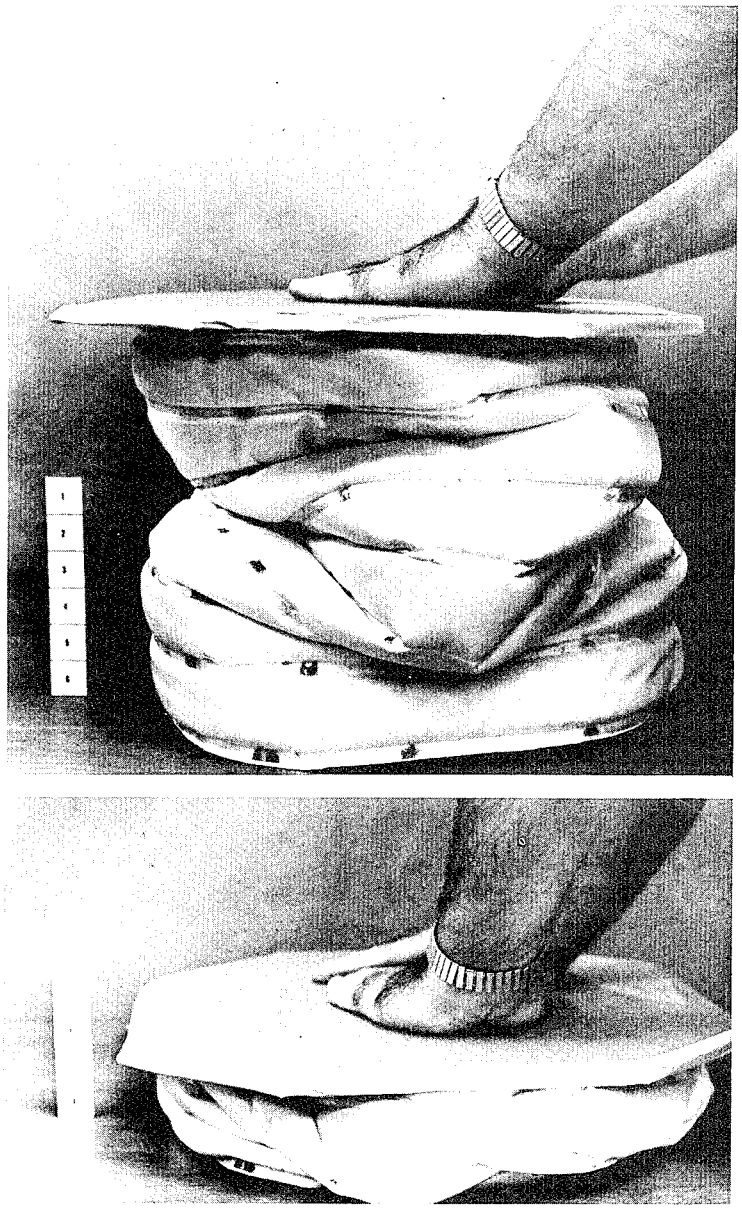

(a)

(b)

Figure 29. Corrugated Cylinder without Bands

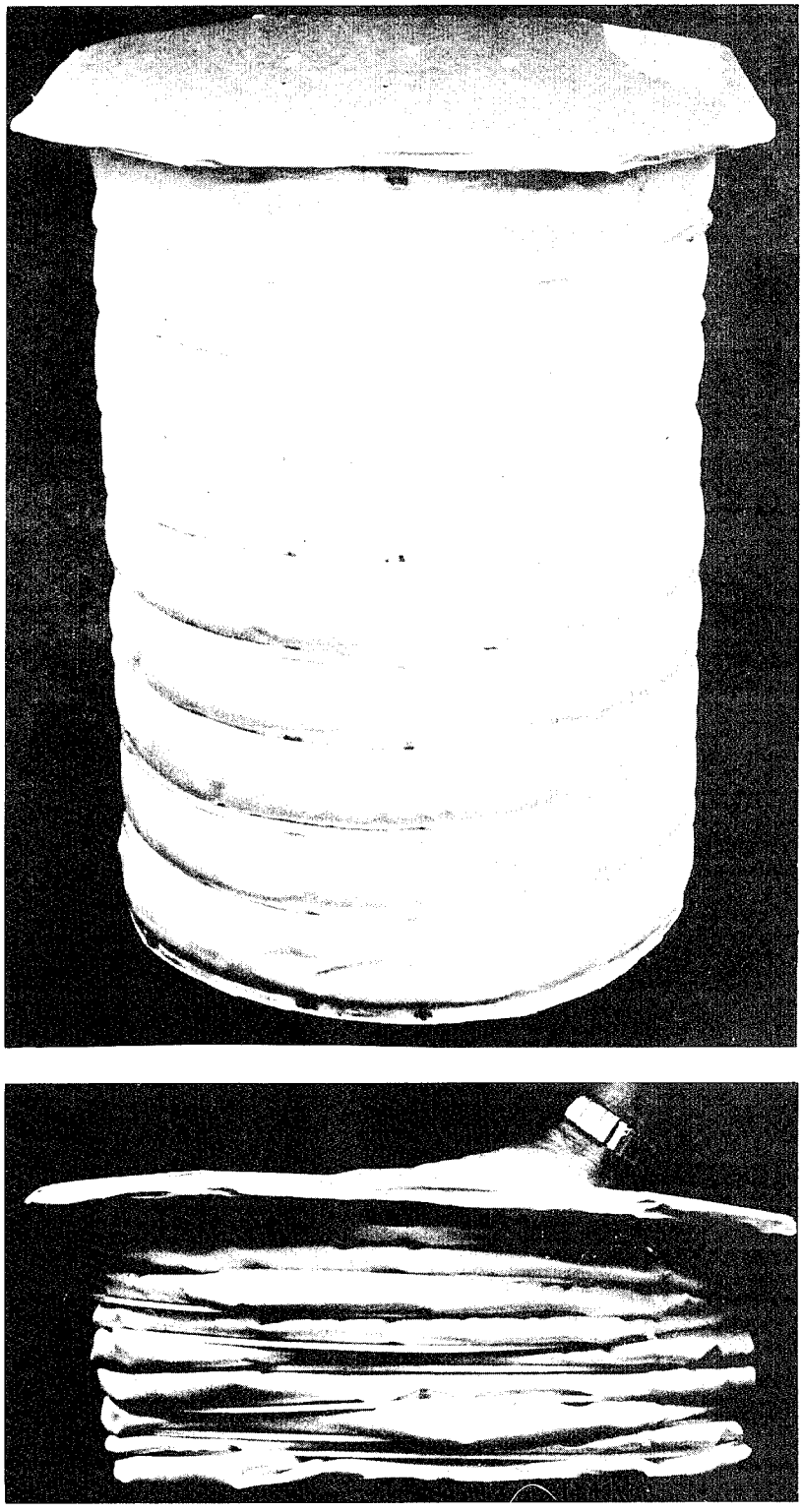

Figure 30. Cylinder Model with Rigid Hoop Rings

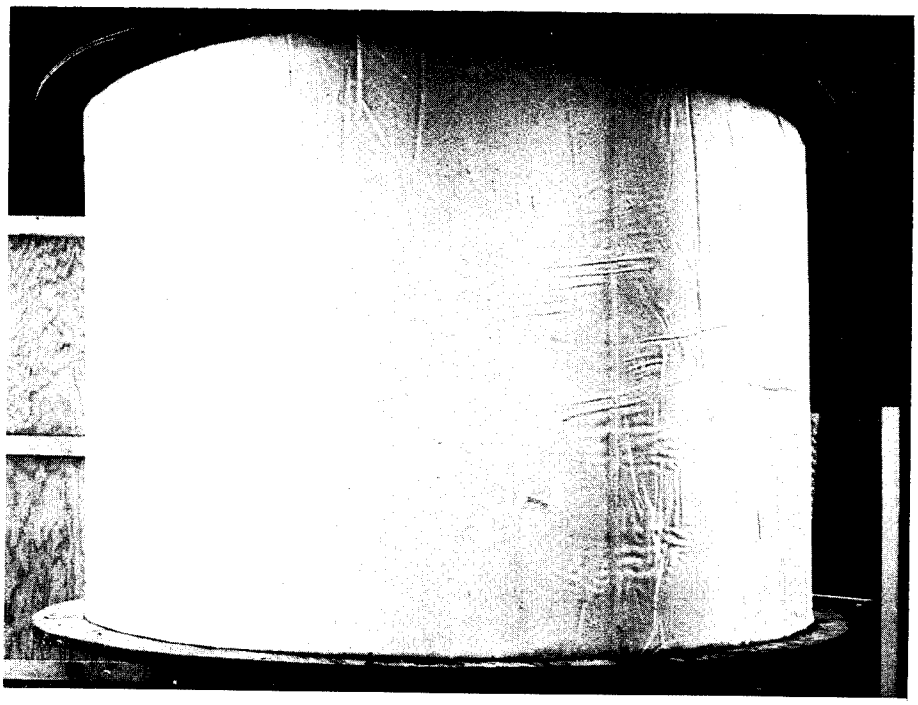

Figure 31. Large Test Cylinder, 4-ft Diameter and 3 ft Long

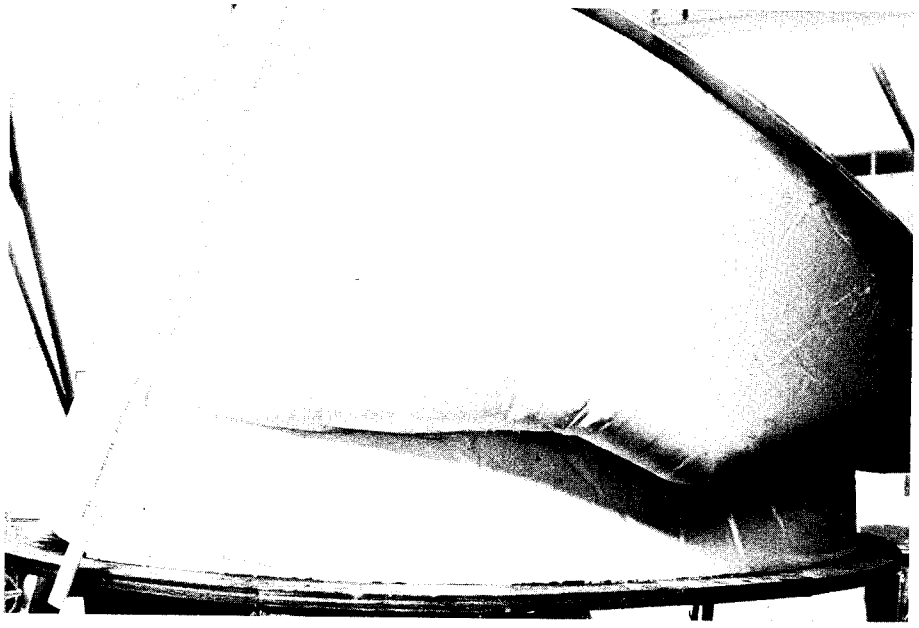

Figure 32. Large Cylinder with Buckling Failure on Initial Test

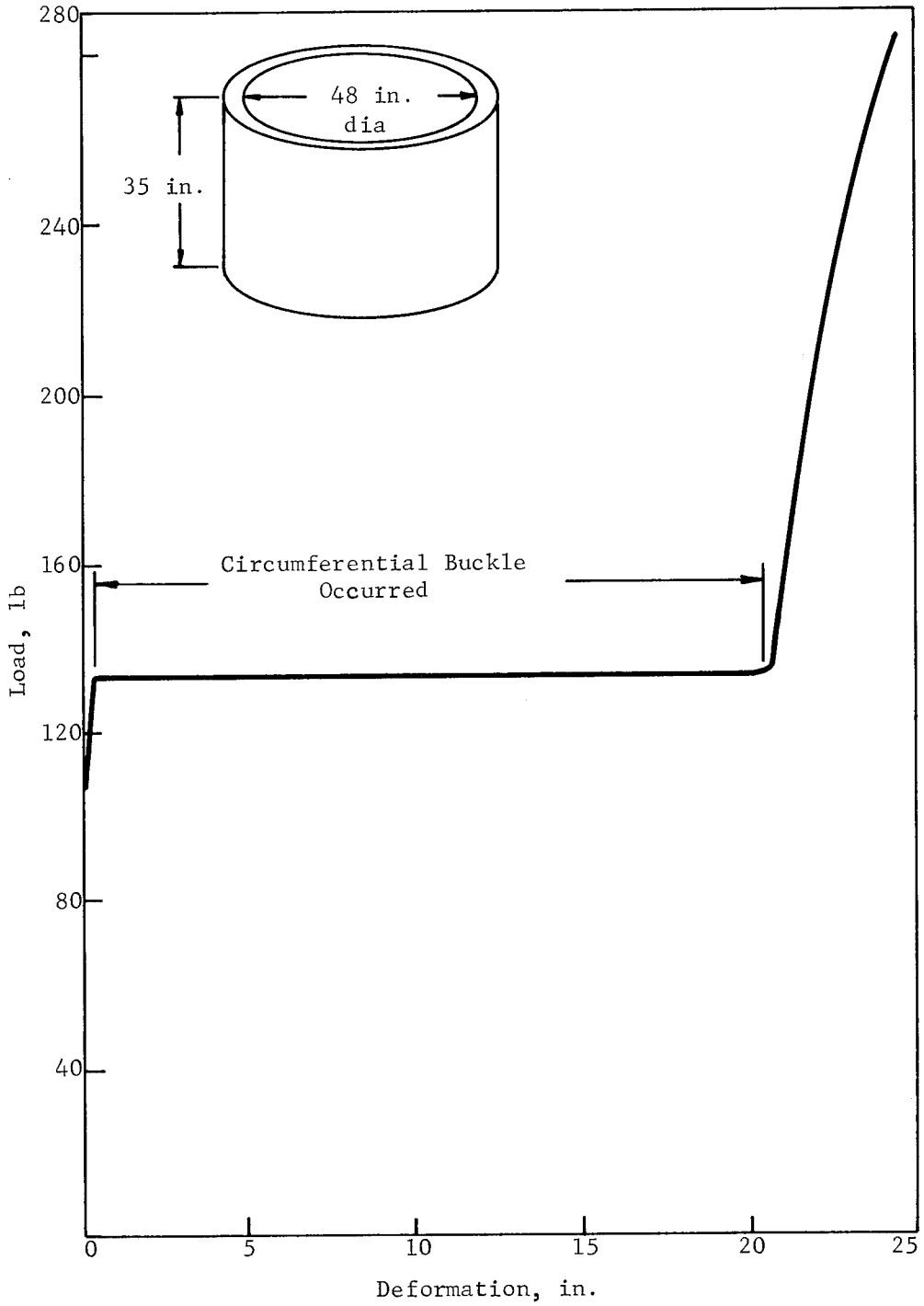

Figure 33. Load-Deformation Curve for 4-ft Diameter Cylinder

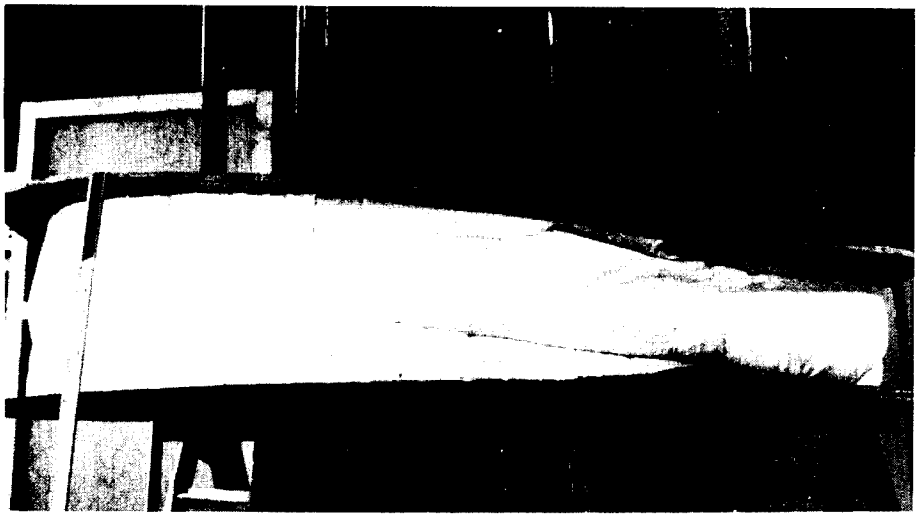

Figure 34. Large Cylinder with Vertical Supports at Maximum Load

Due to the circumferential buckle, the cylinder did not completely return. This test indicates the importance of packaging the cylinder by compression of the material. The circumferential buckle prevented the cylinder from completely returning to its original configuration after the load was removed. It expanded from a compressed height of 8 in. to an unloaded height of 12-1/2 in. in less than 1 minute. Twenty-four hours later, there had been no significant change in height of the cylinder. After this time the buckle was mechanically removed and the cylinder self-deployed to its original height. It is anticipated from the results of the tests conducted with rigid convolution rings that an airlock designed with convolution and rigid rings would compress in a favorable configuration and would fully deploy. However, even if the airlock did not completely deploy, pressurization would complete the deployment. The foam would then recover and maintain this expanded configuration.

A. Packaging Capabilities

Based on data obtained from the cylinder studies, the package ratio for the different configurations was compiled (see Table 8). The first cylinder type gives the optimal condition, where all the material in the wall could be tightly packaged. This volume ratio of 16.4 would also hold for the length ratio of the airlock configuration since the base area of the package area remains constant. However, the airlock structure cannot reach this maximum ratio because the flexible composite wall, when packaged, would leave a void in the center of the package. The second entry in Table 8 gives the packaging ratio based on the test of the 4-ft diameter cylinder. The test data show an expanded-to-packaged ratio of 4.6 based on length measurements. The third packaging ratio of 3.4 given in Table 8 was for a small (1/4 size) cylinder which had "stiff" skins. The skins for this cylinder were impregnated with the polyvinylidene chloride latex. The fourth test cylinder listed in Table 8 was also 1/4 size but utilized the bond skins which resulted in improved composite flexibility. The stiff rings prevented large buckles from forming as shown in Figure 30 and resulted in a packaging ratio of 7.4.

The actual packaging ratio of the airlock would be slightly better than the 7.4 given for the fourth test cylinder in Table 8. This reasoning is based on the fact that the material would be equivalent in flexibility and the spacing between rings would be greater. The true packaging ratio of the cylinder will be known when a full-scale and geometrically correct model is constructed.

TABLE 8

PACKAGING RATIO FOR AIRLOCK TYPE STRUCTURES

Type	Size	Packaging Ratio
1) Test cylinder; internal volume to material volume ratio	4-ft dia; 3 ft high; 2.2 in. thick wall	$\frac{V_{expanded}}{V_{packaged}} = \frac{37.7}{2.3} = 16.4$
2) Test cylinder	4-ft dia; 3 ft high; 2.2 in. thick wall	$\frac{L_{expanded}}{L_{packaged}} = \frac{36}{8} = 4.5$
3) Test cylinder; no rings, "stiff" skin	12-in. dia; 22 in. high; 1 in. thick wall	$\frac{L_{expanded}}{L_{packaged}} = \frac{22}{6.5} = 3.4$
4) Test cylinder; flexible rings, flexible skin	12-in. dia; 22 in. high;	$\frac{L_{expanded}}{L_{packaged}} = \frac{22}{3} = 7.4$

IX. DESIGN OF AIRLOCK

The actual "design" of the expandable structure is dependent on the previously discussed items. The structural fabric established the basic shape required for astronaut egress. The thickness of the meteoroid protection layers have been established. The remaining design aspects include the attachments, hatch mechanism, and the retraction mechanism. The complete airlock design conception is shown in Figure 35. The previously noted items are discussed in detail in the following sections.

A. Attachments

The primary purpose of the attachment is to provide a means for transferring the airlock load to the base structure. The structural end rings for the airlock only require attachment to the load-carrying layer, the structural fabric. The best mechanisn for transferring the load from the structural fabric is by means of a circular rim.

B. Rim

The design load on the rim is given by equation (10) in Section V

$$F_R' = \frac{n\,T}{\pi\, r_D} \cos\,(\alpha_D + \beta)$$

where

$$\beta = \frac{1}{2}\left|\frac{\pi}{2} - \alpha_D\right| = \frac{1}{2}\,(90° - 58.21°) = 15.90°$$

Then

$$F_R' = \frac{19{,}320}{\pi\,(18)} \cos\,(90° - 15.90°) = 93.5\ \text{lb/in.}$$

This load is taken by the rim on a contoured flange, as shown in Figure 36.

The bending stress in the rim which results from the attachment load F_R' can be estimated by considering the load to be supported by radial stresses alone (i.e., by neglecting the contribution from tangential stresses). For this calculation, assume the overhang to be $a = 0.5$ in. Then the radial bending moment is

$$M_R' = F_R'\,a = 93.5\ \text{lb/in.} \cdot 0.5\ \text{in.} = 47\ \text{lb in./in.}$$

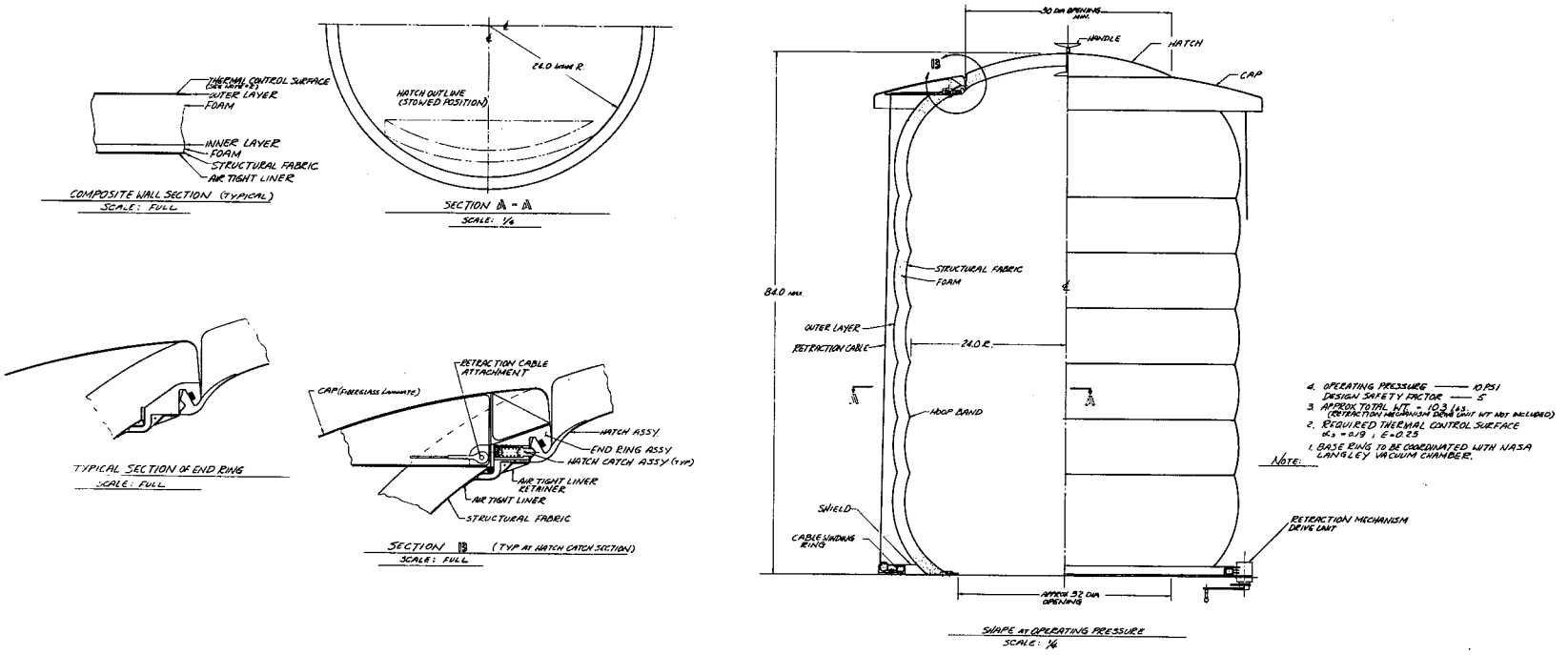

Figure 35. Expandable Airlock General Design Concept

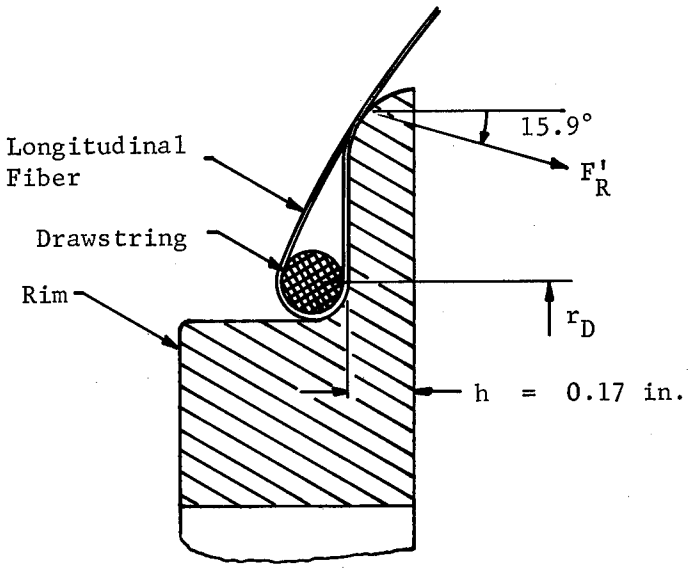

Figure 36. Cross-Sectional Detail for Rim
(Scale: 2 times full size)

The section modulus per inch of rim length is

$$\frac{I'}{C} = \frac{h^2}{6} \text{ in.}^3/\text{in.}$$

where h is the thickness at the root of the flange. For a design stress of 10,000 psi.

$$\frac{I'}{C} = \frac{h^2}{6} = \frac{M'}{S} = \frac{47.}{10,000}$$

or

$$h = 0.17 \text{ in.}$$

Analysis of the attachment of the rim to a base was deferred until this structure is defined. At this time, a bolting circle would be the most convenient, as shown at the base of the airlock depicted in Figure 35.

For the construction of the airlock, the structural fabric with the drawstring in place would be held in contact with the rim by means of a clamping ring. The same method of attachment will be used at the hatch end of the airlock, and the clamping ring is shown in hatch end detail of Figure 35.

C. Hatch

The hatch for the expandable airlock concept presented some design problems, due to the nature of the flexible structure. It was assumed throughout this study that a rigid hatch would be used for the airlock. Other basic design criteria included the following:

1. The hatch would have a positive seal; i.e., the seal would become tighter when under pressure.

2. An opening load of 40 lb or less was desired.

3. Hinges would not be used because of the flexible nature of the wall.

The result of these criteria was a hatch with a spherical radius which combined the catching and sealing functions in a single unit. The basis of the design was the premise that the astronaut would be able to pull the hatch toward himself more easily than applying a torsion. Hence, the hatch was designed to open inwardly, which would also provide the positive seal. The hatch would be held in place with bullet-type catches spring-loaded to provide the force to hold the hatch in place. It was estimated that three catches would hold the hatch in place. A load of 30 lb was estimated as the requirement to open the hatch with a zero pressure differential. A section of the hatch ring and catches are shown on the face of the conceptual drawing (see section B of Figure 35).

The spherical shape of the hatch was chosen to allow for a general membrane type stress field in the shell of hatch. Areas of discontinuity would occur, however, around the edge of the shell. The edge rings will provide edge restraint in this area. The hatch edge ring was tapered to prevent a stiffness discontinuity in the transition between the metal ring and the laminate shell.

The spherical hatch shell was assumed to be an omnidirectional, rigid glass reinforced plastic laminate to provide both high strength and low weight. The analysis of omnidirectional laminate strength levels was obtained from the procedure given in MIL-HDBK-17 (Reference 14). The analysis accounts for the effect of layers of cloth plied at different angles. From this work, the minimum strength would be 29,000 psi. This configuration was found to be lightest weight construction. For example, this laminate would weigh approximately 2 lb, while a flat sandwich panel for the same loading condition would weigh a minimum of 7.4 lb. The flat sandwich panel weight was based upon the design procedure outlined in MIL HDBK-23 (Reference 15) for the loading condition of uniform pressure for flat, circular panels.

This type of spherical hatch which combines the catching and sealing functions on the outer ring would provide the best performance for closure attachment to the flexible airlock.

To provide protection from the micrometeoroid environment, the top of the hatch would have the foam and bumper layers equivalent to the protection afforded the flexible wall.

D. Retraction Mechanism

The requirement for deployment – retraction cycles necessitated the use of a retraction mechanism for the expandable airlock. Use of flexible cables was the most effective method of retracting the airlock. The cables were attached to the top ring of the airlock, and spacers were used to locate the cables away from the outer surface of the flexible material. The space between the cable and wall material would prevent rubbing of the thermal control surface by the cables.

The winding ring device was devised as an adequate system of reeling in the cables for airlock retraction after evaluating several systems. Two of the systems investigated and discarded in favor of the winding ring were a torque cable and bundling of the retraction cables. The latter system was the simplest since all the retraction cables were gathered together at a single drum. The primary disadvantage for this system was the possibility of the cables fouling on each other. The torque cable system consisted of a series of drums around the circumference of the airlock base. A retraction cable was mounted on each drum. The drums were interconnected by the torque cable which provided the turning force. This system was discarded due to the unequal loads which would be applied to the cables.

It was desired to have a retraction mechanism which applied an equal load to all cables, required a minimum of space station modification, was simple to maintain, and, of course, was lightweight. The winding ring appeared to fit these requirements. The winding ring concept is shown in Figures 1 and 35. In operation, the retraction cables are all mounted to the ring to provide equal tension. As the ring rotates, the cables would be wound on the ring and the airlock pulled in. The torque to provide the rotation would be applied by a drive unit which could be either motorized or manually operated. The power requirements for the retraction mechanism would be relatively small due to the torque multiplication of the large diameter ring. This system had the advantage in that it required only a single hole through the spacecraft wall for the drive shaft, which reduces the number of possible leak areas to a minimum.

E. Inner Liner

The inner liner is the primary gas barrier for the airlock system. As discussed previously, 2-mil thick polyvinylidene chloride would be adequate for this purpose. The liner is not attached to the structural fabric but sealed at each end ring. The liner would be fabricated to the shape (i.e., convolutions) the airlock assumes with operating pressure.

Since the liner is not attached to the structural fabric, provisions for replacing the liner, should this become necessary, have been incorporated into the airlock design. The ends of the liner would be formed into seals which in turn would fit into the end rings. An alternative to the replacement liner would be to add more material to the liner to provide a "scuff" surface. This approach would simply add to the reliability of the single liner. Either method would probably result in the same weight penalty.

X. WEIGHT ESTIMATE

The weight estimate for the expandable airlock system is shown in Table 9. Not included in this weight estimate were the valving system, retraction ring drive unit, and a base closure plate. These items require a system analysis which was beyond the scope of this feasibility study. The wall of the airlock was based upon an assumed area of 95 sq ft. The material weight for the wall was based upon the weight of actual composite samples and structural fabric which resulted in a total of 43.4 lb. The end rings, hatch, hoop rings, and inner liner accounted for 41.8 lb. The remainder of the 101-lb airlock system weight consisted of the retraction mechanism.

TABLE 9

AIRLOCK WEIGHT ESTIMATE

Item*	Materials	Wt., lb
1. Hatch	Laminate, ring & foam	10.5
2. Upper end ring	Aluminum	18.9
3. Cap	Laminate	3.0
4. Composite wall**		
a. Protection layers b. Structural fabric	Foam & cloth 38 lb Dacron & monofilament 5.4 lb	43.4 (total)
5. Hoop rings and drawstrings (2)	Wound fiberglass	6.5
6. Airtight liner	Polyvinylidene chloride	2.5
7. Bottom end ring	Aluminum	3.4
8. Retraction mechanism	Various	
a. Cable hanger (4)		4.0
b. Cables & eyes (4)		1.0
c. Pulleys (8)		0.8
d. Winding ring		4.0
e. Winding ring retaining assembly (4)		1.0
f. Shield assembly	Laminate	2.0
	Total Wt.	101.0

* Valves, tubing, retraction drive unit, or attachment plate not considered.

** Composite wall weight based on a surface area of 95 ft^2.

XI. CONCLUSIONS AND RECOMMENDATIONS

From this program, the following items for the expandable airlock concept were established:

1. The flexibility required for sufficient packaging was obtained.

2. The required optical properties for the thermal control coating have been established which, along with the insulation properties of the foam, provide the necessary thermal protection from the maximal heating condition.

3. The protection necessary from the expected micrometeoroid environment has been determined.

4. The hatch preliminary design was established to meet the leakage and opening requirements.

5. The retraction system was designed for the airlock repackagability requirements.

Narmco recommends that a full-scale operational expandable airlock be fabricated and evaluated for possible use on a further space mission. The related work to this task would include the final design of the attachment rings and retraction mechanism. Determining the thermal control coating, which would have the proper values, must also be included in the future endeavor.

REFERENCES

1. Whittaker Corporation, Narmco Research & Development Division, Development and Evaluation of the Elastic Recovery Concept for Expandable Space Structures, Final Report, by N. O. Brink et al., Contract NASw-661, San Diego, Calif., 29 Apr 1964 (also NASA Contractor Report CR 121, Dec 1964)

2. John L. Mason, Ph.D., "Spacecraft Thermal Management" (lecture presented as part of course given at UCLA, Los Angeles, Calif., May 1964)

3. F. Kreitm, Principles of Heat Transfer, International Textbook Company, Scranton, Pa., 1958

4. D. L. Clemmons and J. D. Camp, "Amorphous Phosphate Coatings for Thermal Control of Echo II" (paper presented at the Multilayer Systems Symposium of the Electrochemical Society, Los Angeles, Calif., May 1962)

5. Air Force Systems Command, Nonmetallic Materials Laboratory, Improved Organic Coatings for Temperature Control in a Space Environment, by H. H. Hormann, Technical Documentary Report No. ASD-TDR-62-917, Wright-Patterson Air Force Base, Ohio, Feb 1963

6. Society of Automotive Engineers, Inc., Aero-Space Applied Thermodynamics Manual, New York, N.Y., Jan 1962

7. Astro Research Corporation, Design of Inner Pressure Shell for Airlock Structure, by J. A. Loisch, ARC-R-159, Santa Barbara, Calif., 15 Aug 1964

8. Astro Research Corporation, Structural and Folding Analysis of the Airlock, by H. Schuerch and A. Kyer, ARC-R-169, Santa Barbara, Calif., 16 Oct 1964

9. Astro Research Corporation, Analysis of Axisymmetric, Rotating Pressurized Filamentary Structures, by O. R. Burggraf and H. Schuerch, ARC-R-74, Santa Barbara, Calif., Sept 1962

10. P. F. Byrd and M. D. Friedman, Handbook of Elliptic Integrals for Engineers and Physicists, Lange, Maxwell, & Springer, 1954

11. Meteoroid data (unpublished) from Systems Engineering Group, Research and Technology Division, Air Force Systems Command, United States Air Force, Wright-Patterson Air Force Base, Ohio

12. National Aeronautical and Space Administration, Meteoroid Effects on Space Exploration, NASA TND 1839, Oct 1963

13. J. H. Gehring, D. R. Christman and A. R. McMillan, "Hypervelocity Impact Studies Concerning the Meteoroid Hazard to Aerospace Materials and Structures" (paper presented at the AIAA Meeting Palm Springs, Calif., Apr 1964)

14. MIL-HDBK-17, "Plastics for Flight Vehicles," Part I Reinforced Plastics, Armed Forces Supply Support Center, 1959

15. MIL-HDBK-23 Part III, "Composite Construction for Flight Vehicles," Part III, Design Procedures, Armed Forces Supply Support Center, Nov 1959

"The aeronautical and space activities of the United States shall be conducted so as to contribute . . . to the expansion of human knowledge of phenomena in the atmosphere and space. The Administration shall provide for the widest practicable and appropriate dissemination of information concerning its activities and the results thereof."

—NATIONAL AERONAUTICS AND SPACE ACT OF 1958

NASA SCIENTIFIC AND TECHNICAL PUBLICATIONS

TECHNICAL REPORTS: Scientific and technical information considered important, complete, and a lasting contribution to existing knowledge.

TECHNICAL NOTES: Information less broad in scope but nevertheless of importance as a contribution to existing knowledge.

TECHNICAL MEMORANDUMS: Information receiving limited distribution because of preliminary data, security classification, or other reasons.

CONTRACTOR REPORTS: Technical information generated in connection with a NASA contract or grant and released under NASA auspices.

TECHNICAL TRANSLATIONS: Information published in a foreign language considered to merit NASA distribution in English.

TECHNICAL REPRINTS: Information derived from NASA activities and initially published in the form of journal articles.

SPECIAL PUBLICATIONS: Information derived from or of value to NASA activities but not necessarily reporting the results of individual NASA-programmed scientific efforts. Publications include conference proceedings, monographs, data compilations, handbooks, sourcebooks, and special bibliographies.

Details on the availability of these publications may be obtained from:

SCIENTIFIC AND TECHNICAL INFORMATION DIVISION

NATIONAL AERONAUTICS AND SPACE ADMINISTRATION

Washington, D.C. 20546